ANALYSIS OF INHERENT ANISOTROPY IN ASPHALT CONCRETE MIXTURES

ZEKARIYAS MUSSIE AMANU

MASTER OF SCIENCE

ADDIS ABABA SCIENCE AND TECHNOLOGY UNIVERSITY

FEBRUARY 2020

ADDIS ABABA, ETHIOPIA

ANALYSIS OF INHERENT ANISOTROPY IN ASPHALT CONCRETE MIXTURES

BY

ZEKARIYAS MUSSIE AMANU

ADVISOR

HABTAMU MELESE ZELELEW

A Thesis submitted to the College of Civil and Architecture Engineering, School of Graduate Studies, Addis Ababa Science and Technology University in Partial Fulfillment of the Requirements for the Degree of Master of Science in Civil Engineering (Road and Transport Engineering).

ADDIS ABABA SCIENCE AND TECHNOLOGY UNIVERSITY

FEBRUARY 2020

ADDIS ABABA, ETHIOPIA

Certificate

This is to certify that the thesis by **Mr. Zekariyas Mussie Amanu**, entitled **"Analysis of Inherent Anisotropy in Asphalt Concrete Mixtures"** and submitted in fulfillment of the requirements for the Degree of **Master of Science** complies with the regulations of the University and meets the accepted standards with respect to originality and quality.

Date of Defense: 5 February 2020

Principal Advisor:

Habtamu M. Zelelew (PhD, PE) — Advisor — Signature — 03/02/2020 — Date

Members of Examining Board:

Dr. Wubishet Jekale — External Examiner — Signature — 11/02/20 — Date

Dr. Melaku Sisay — Internal Examiner — Signature — 12/03/20 — Date

Dr. Melaku Sisay — ERA, PG Program Coordinator — Signature — 12/03/20 — Date

Mr. Alemayehu Feyissa — Head, Civil Engineering Department — Signature — 12/03/20 — Date

Dr. Sisay Demeku — Dean, College of Architecture and Civil Engineering — Signature — 08-06-2020 — Date

Declaration

I certify that research work titled, **"Analysis of Inherent Anisotropy in Asphalt Concrete Mixtures"** is my own work. The work has not been presented elsewhere for assessment. Where material has been used for other sources, it has been properly acknowledged.

Name: Zekariyas Mussie Amanu

Signature: Zek'M

Date of Submission: 11 Mar. 2020

Acknowledgment

Firstly, I would like to express my sincere thanks to my advisor Dr. Habtamu Melese, who has supported me throughout my thesis work and sacrifices his valuable times to encourage me, to work in my own way. Dr. Habtamu, is a great advisor and it would not have been possible to achieve the ultimate target of this study without valuable helps.

Many thanks to the Ethiopian Road Authority (ERA) for giving and granting me this opportunity. In addition, I would like to extend many thanks to Addis Ababa Science and Technology University (AASTU) especially to all the members of college of Civil and Architectural Engineering, Civil Engineering Department.

Last but not least, many thanks to all my colleagues and friends for valuable help and support.

Abstract

Asphalt Concrete mixtures were characterized by one of mechanistically modeling technique, inherent anisotropy of the material. The performance of AC mixtures is influenced by the arrangement of aggregates and their associated air voids. The main objective of this study to analyze aggregate orientation and evaluates inherent anisotropy in AC mixtures using X-ray CT images by means of microstructure parameter. There are three AC mixture designs: coarse graded CMHB Type C, gap graded PFC and fine graded Superpave Type C AC mixtures. They are prepared with hard limestone aggregate and compacted with SGC, having a PG 76-22 modified binder.

Digital image processing algorithm is adopted for this study to process X-ray CT scanned images and effectively separate the connected or overlapping aggregates using *MATLAB*® 2018b, image processing toolbox. It includes for both coarse and fine aggregate particles ranging from 1.18 mm to 19 mm. The aggregate orientation, size and area can be used to define internal structure parameters (i.e., modified Vector magnitude) to evaluate inherent anisotropy of AC mixtures.

Aggregates have three dominant average orientations having 20% of the aggregates has an inclination angle between (-10^o-10^o), 65% of the aggregates have an inclination angle between (-45^o-45^o) and 15% of aggregates have an inclination angle between (-45^o-90^o) for three AC mixtures. Small inclination angle indicates the aggregates lies flat in the horizontal direction that is perpendicular to the compaction direction. In addition, statistical analysis was performed for AC mixtures within AC layers. It results, aggregate orientation varies within AC layers. Variation of aggregates orientation is performed using Scheffe multi-comparison test.

Vector magnitude is an internal microstructural index, which is used to quantify the average inherent anisotropy of AC mixtures. For three AC mixtures; a Vector magnitude doesn't exceed a value of 0.25 as well as modified Vector magnitude value of 0.6. The composition of aggregates for CMHB Type C is coarse, for PFC is a gap and for Superpave Type C is fine graded aggregates. Due to this, for three AC mixtures; CMHB Type C has greater microstructural parameter than PFC and Superpave Type C AC mixtures.

Based on the results, the undamaged zero month aging AC mixtures was inherently anisotropic. Aggregate morphological properties (i.e., orientation, area and aspect ratio) increase microstructural parameter than considering only orientation of aggregates to quantify inherent anisotropy of AC mixtures. It indicates that the Vector magnitude substantially underestimates the inherent anisotropy of the AC mixtures. The study include challenges in visualizing images as matrix form, creating what if scenarios, executing algorithm and identifying causes of algorithm failure in $MATLAB^{®}$ software. The future scope may include; varying compaction level and angle of gyration, changing compaction methods, using aging AC mixtures, varying image resolution and specimen height.

Keywords : Asphalt Concrete, Aggregates, inherent anisotropy, orientation, internal structure, Vector magnitude, X-ray CT images.

Contents

List of Figures

List of Tables

List of Symbols

Δ	Vector Magnitude
Δ'	Modified Vector Magnitude
F_{ij}	Microstructure Tensor
P_b	Percent binder Content
V_a	Percent air Voids
$E(m)$	Probability Density Function
C_{ijkl}	Elastic Modulus Tensor
δ_{ij}	Kronecker Delta
Ω	Solid Angle
θ_k	Orientation for the K^{th} Aggregate particle
θ	Aggregate Orientation
μ	Experimentally determined parameter
D_2	Second invariant of the deviatoric Fabric Tensor
λ^k	Aspect ratio of the k^{th} Aggregate particle
ρ^k	Area of the k^{th} Aggregate particle
q	Maximum Modulus ratio

List of Abbreviations

AACRA	Addis Ababa City and Road Authority
AASHTO	American Association of State Highway Transport Officials
AC	Asphalt Concrete
ASTM	American Society of Testing Materials
CMHB	Coarse Matrix High Binder
CT	Computed Tomography
DEM	Discrete Element Method
DIP	Digital Imaging Processing
DOT	Department of Transportation
DSR	Dynamic Shear Rheometer
ERA	Ethiopian Road Authority
FDM	Finite Discrete Method
FEM	Finite Element Method
HMA	Hot Mix Asphalt
PFC	Porous Friction Coarse
PG	Performance Grade
RTFO	Rolling Thin Film Oven
SGC	Superpave Gyratory Compactor
SSB	Sum of Squares Between Groups
SST	Sum of Squares Total
Superpave	Superior Performing Asphalt Pavement
VGM	Volumetric-based Global Minima
VFA	Percent Voids Filled with Asphalt
VMA	Percent Voids in Mineral Aggregates

Chapter 1

Introduction

1.1 Background of the Study

Asphalt Concrete is a composite material which consists of Aggregates, Mastics (i.e., binder and filler) and air voids. Mastics are blends of asphalt binder and fine particles, typically considered as particles passing sieve No. 200 (i.e., sizes finer than 75 μm) [29]. AC homogeneity is dependent on the distribution of its components among which aggregate distribution plays an important role, because the distributions of the other components in AC mixtures are usually determined by the aggregate distribution [7]. The proportions, distribution and interactions of these three phases define the micromechanical behavior of AC pavements. To date, microstructure plays a significant role in modeling and simulation of different behavior of AC mixtures.

Aggregates are the principal load supporting components of AC Pavement. Aggregates constitute 75-85% of the mixture by volume and 90-95% of the mixture by weight [31]. They are mixed with 5-10% asphalt cement to form AC. The load carrying capacity of AC comes primary from aggregate-to-aggregate interlocking and contact friction. Hence, morphological properties of aggregates have long been recognized as critical factor in influencing the structural and functional performance of AC mixtures [8, 21]. Compaction methods and loading conditions also affect the way how aggregate particles align in the horizontal plane. During compaction, the orientation of aggregate particles continuously changes due to the applied pressure and number of gyration.

Anisotropy of an AC mixture is defined as a difference in physical properties, such as modulus ratio, when the AC mixture is measured in different directions. Inherent anisotropy in granular materials exists due to anisotropic compaction, restrain conditions and gravity direction even before the pavement is subjected to traffic. Stresses due to construction operations and traffic create anisotropy and new particle contacts are formed due to breakage and slippage of particles, which induces further anisotropy.

The inherent anisotropy due to preferentially oriented aggregates was characterized by a microstructural parameter (i.e., vector and modified vector magnitudes) which could be rapidly and accurately measured by lateral surface scanning tests and physically related to anisotropic modulus ratio.

Realistic determination of orientation distribution of aggregate particles and in turn vector magnitude requires 3D scanning of AC mixtures. To date, development of high resolution imaging technique such as X-ray computed tomography (CT) was provided for Pavement Engineers with superior tools to capture and characterize the microstructure of AC mixtures.

High resolution X-ray CT is a non-destructive advanced imaging technique that generates 2D and 3D high-resolution images with the capability of capturing the details of the microstructure. It allows the study of variety of AC mixture properties, including aggregate orientation, segregation and anisotropy. Images was processed using $MATLAB^{®}$ 2018b, image processing toolbox software.

Previously, destructive techniques that involved cutting the AC specimen in equally spaced sections or scanning the outer surface of the specimen along with the assumption of randomness to obtain the 3D distribution from the 2D measurements was done. As a result, such processes have proven to be time consuming and subjective. Much research had been done on AC mixtures mainly concentrated on the macroscopic properties (i.e. aggregates > 2mm size) [32, 37]. Mechanistic models mainly concentrated on the macroscopic behavior of AC mixture using principle of continuum mechanics of the composite materials based on the assumption that the mixtures are homogeneous and isotropic [17].

Innovative measures based on image processing to quantify the internal structure of AC mixtures was presented in the paper. Measures are developed to analyze aggregate orientation and evaluates inherent anisotropy in AC mixtures. It presents for both coarse and fine aggregate particles ranging from 1.18 mm to 19 mm using an aggregate related geometric parameter, the modified vector magnitude with the support of X-ray CT images.

1.2 Statement of the Problem

Pavement distresses (i.e., Rutting, shoving and segregation) mainly depend on the Aggregate morphological characteristics. The mechanical performance of AC mixtures is influenced by the properties of aggregate blends (i.e., grading, shape (angularity and elongation) and texture (roughness)). Rutting defined in ASTM standard E867 as "a contiguous longitudinal depression deviating from a surface plane defined by transverse cross slope and longitudinal profile". It is rated as the most significant distress type regarding damage in pavements mainly in hot climates. Rutting would be underestimated without including the inherent anisotropy in the constitutive modeling [37].

Aggregate properties and compaction methods of the micromechanical behavior wasn't addressed briefly in the design of AC mixtures. During compaction, orientation of aggregate particles is continuously changing due to the applied pressure and number of gyrations. The density or percent air voids of HMA are currently the most accepted quality control parameter for AC pavements. Several studies show that AC mixtures with similar density can exhibit very different response to loading. Due to this, it is necessary to find alternative means to quantitatively determine sufficient level of compaction and resistance to loading to minimize rutting of AC mixtures.

Current pavement design philosophy in Ethiopia is an Empirical approach. Due to this, we can improve our design philosophy from Empirical approach to Mechanistic Empirical Pavement Design Guide. Characterizations of an AC mixtures include two parts: nondestructive and destructive characterization of the material properties. Among the two, inherent anisotropy of AC mixture is included within the nondestructive characterization of material properties that is caused by the preferential orientation of aggregates. The following issues occur when we characterize the inherent anisotropy for the AC mixtures;

- A nondestructive imaging system with high resolution is required to obtain the aggregate properties of the AC mixtures.
- Orientation of aggregates was considered, for both coarse and fine aggregates. In the continuum mechanistic modeling, inherent anisotropy is accounted for in the viscoelastic and the viscofracture characterization of AC mixtures.

1.3 Research Questions and Hypothesis

Permanent deformation and fracture are two major distresses of AC pavements. Different aggregate structures within AC mixtures can be sufficiently characterized by three internal structure indices: orientation, number of contact zones and contact length per area. Before beginning, aggregate morphological properties such as: area, equivalent diameter, perimeter, major axis length, minor axis length, and orientation were addressed.

- Major axis inclination of horizontal axis was used to determine the orientation, which in turn, used to index the Vector magnitude of aggregate particles.

Depending on the above, the following research gaps were arise;

- Is there any effect on aggregate orientation of AC mixtures due to constant compaction pressure?
- Is there any relation between Fundamental properties (modulus, E) and AC mixture parameters?

Depending on the above questions and factors, the fundamental hypothesis in this research was, the internal structure indices, like aggregate morphological characteristics are better descriptive parameters than volumetric properties for characterizing the inherent anisotropy of AC mixtures that have more resistance to rutting results in long lasting pavements and enhanced performance. In addition, having constant compaction pressure AC mixtures aggregate orientation vary throughout the specimen height.

1.4 Objective

1.4.1 General Objective

The general objective of this research is to analyze aggregate orientation and evaluates inherent anisotropy of AC mixtures using an aggregate related geometric parameter, modified Vector magnitude with the support of X-ray CT images.

1.4.2 Specific Objectives

Specific objectives of this research are:

- To evaluate AC mixtures microstructure properties using image analysis.
- To utilize microstructure parameters (Δ and Δ') in studying the inherent anisotropy of AC mixtures.
- To evaluate the effects of Δ' on the fundamental properties (i.e., modulus, E) of the AC mixtures.

1.5 Scope of the Study and Significance

In this study, particular emphasis was on the analysis of aggregate orientation and evaluates inherent anisotropic properties of AC mixtures from the other mechanistically modeling techniques (i.e., viscoelasticity, viscoplasticity and viscofracture) by using an aggregate related geometric parameter, the modified Vector magnitude. To evaluate inherent anisotropy of AC mixtures, aggregate morphological properties (i.e., orientation, area and aspect ratio) are considered. The three AC mixture designs are: Coarse Matrix High binder (CMHB) Type C, Porous Friction Course (PFC) and Superpave Type C.

High Resolution X-ray CT are considered to scan and evaluate microstructure properties using image analysis for AC mixtures. Using scanned X-ray CT images, microstructure parameters (Δ and Δ') are considered in studying the inherent anisotropy of AC mixtures. In addition, to evaluate the effects of Δ' on the fundamental properties (i.e., modulus, E) of the AC mixtures. Performance of a given Pavement includes; structural and functional performance. They are affected by aggregate morphological properties. Due to this, Highway Agencies can use this research to construct well designed and economically safe roads.

1.6 Thesis Organization

The thesis was written according to the guidelines provided in the Addis Ababa Science and Technology University Thesis Manual. The organization of this study includes the following chapters. The first chapter presents an introduction to the research topic which contains background information, a statement of the problem, objectives, hypothesis, scope of the study and thesis organization. The second chapter presents on a brief review of literatures on previous research that used aggregate orientation and evaluates inherent anisotropy in AC mixtures, which includes, methods for measuring the internal structure anisotropy of granular materials, X-ray CT scanning and Image Processing, aggregate orientation and vector magnitude.

The third chapter presents on backbone of this research methodology and materials used. The fourth chapter presents on results and discussion. Primarily, image analysis results on orientation, internal structure parameter with relationship of AC parameters (i.e., modulus ratio, E). The conclusions and recommendation for future study are given in chapter five.

Chapter 2

Literature Review

2.1 Introduction

Asphalt Concrete is a composite material which consists of Aggregates, Mastics (i.e., blends of asphalt binder and fine particles) and air voids. It is composed of approximately 5% air void, 12% binder or mastics and 83% aggregates plus fillers by volume while 5% air void, 5% asphalt binder and 90% aggregates plus fillers by mass [29]. It is a Viscoplastic material. Its internal structure is anisotropic, which could be due to the anisotropic particle and void shape, particle orientation distribution and anisotropic compaction (restrain and force pattern applied during the compaction). Unbound granular materials display significant anisotropy because of non random distribution of particles [18, 19]. However, the majority of the current mechanical tests and analytical models for AC mixtures are based on the assumptions of isotropic material properties.

Nowadays, several researchers implemented Image Processing techniques and have gained in characterizing the microstructure of AC mixtures [12, 25, 32, 35]. Quantitative results clearly indicates the microstructure characteristics of coarse aggregates in AC mixtures: gradation of aggregate by the feret diameter gives an excellent prediction of coarse aggregates ($\geq 2mm$). Inherent anisotropy of AC mixtures was investigated using a modified Vector magnitude that accounts for key aggregate characteristics (i.e., orientation, area, and sphericity) by [37].

Aggregate Orientation is affected by the compaction methods and loading conditions. During compaction, the orientation of aggregate particles continuously changes due to the applied pressure and number of gyrations. The anisotropy of the modulus and Poisson's ratio increases as the pressure loading on the asphalt mixture increases [27]. Compared to the modulus, Poisson's ratio due to air voids has been shown to be more anisotropic. Due to this, the maximum of Poisson's ratio and modulus is shown to be up to 80% and 11% higher than the minimum, respectively.

Image processing is the technique to convert an image into digital format and perform operations on it to get an enhanced image or extract some useful information from it. This chapter overview analysis of aggregate orientation and evaluates inherent anisotropy of the AC mixtures in terms of the size, orientation and sphericity of aggregate particles and void spaces. The internal structure of the aggregates in the AC mixtures are formulated using aggregate related geometric parameter, vector magnitude with the support of X-ray CT images.

2.2 Hot Mix Asphalt

Depending on the mixing process and the temperatures that are used, the asphalt will be considered Hot, Warm and Cold mix asphalt. All asphalt is a mixture of coarse aggregate, fine aggregate and petroleum based asphalt cement. Among the three; Hot mix asphalt is considered for this study. Hot mix asphalt is heated and poured at temperatures ranging from 300-350^oF. It is a flexible mix that is highly weather resistant and able to repel water. The volumetrics and aggregate gradation has a direct effect on their performances and significantly influence the rutting resistance behaviour of AC mixtures.

2.2.1 Permanent Deformation of AC Pavements

Rutting is considered to be one of the most serious distress in AC pavements mostly in hot climates. It is a surface depression along wheel paths caused by the plastic deformation of the AC materials. It is gradual process and occurs in their early life. The contribution of the AC layer to rutting is significant compared to the contribution of the other pavement layers (i.e., base, subbase and subgrade). Rutting is caused by a combination of densification (decrease in volume and hence increase in density) and shear deformation. Later case, may occur in any or all pavement layers, including the subgrade. The former is due to the action of wheel loads along the wheel paths. Researchers suggests that shear deformation rather than densification is the primary rutting mechanism [24].

The interaction of air void-mastic-aggregate affects greatly on the permanent deformation behaviour of AC pavements. For example, at higher pavement temperature, the viscosity of binder tends to decrease, yielding less rutting resistance. Over-estimation of the air voids leads to aggregate segregation that results higher permanent deformation. In addition, having higher binder content (in order to decrease air void) leads an increase in permanent deformation. The permanent deformation of AC mixtures is highly dependent on the testing methods, specimen preparation procedures, testing temperature, stress level and loading time.

Laboratory tests are performed to characterize the permanent deformation behaviour of AC mixtures. These include: (1) Uniaxial Creep and repeated and repeated tests (2) triaxial creep and repeated tests (3) hollow cylinder tests, and (4) simple shear tests. Selection of a particular testing method depends on the cost of equipment, the simplicity of the testing procedures, and the material response. Simple shear tests are realistically suitable to simulate AC rutting as the shear deformation is the dominant cause and failure mechanism of AC rutting. The unconfined static Uniaxial creep tests are recommended to characterize AC mixture permanent deformation behaviour [33].

Numerical modelling and simulation of the permanent deformation behavior of AC pavements are done using continuum, micromechanical and continuum-micromechanical approaches. The continuum based numerical models predict the macroscopic stress-strain response of the material, assuming continuity in displacements. It includes Finite Element Method (FEM), Finite Difference Method (FDM) and Boundary Element Method (BEM). Micromechanical models allow finite displacements and rotations of circular particles to simulate their interactions within the stressed granular assembly. Discrete Element Method (DEM) is a numerical simulation modeling technique, commonly for granular and rock materials. Figure 2.1, shows the influence of Anisotropy on Stress-Strain relationship using micromechanical approach.

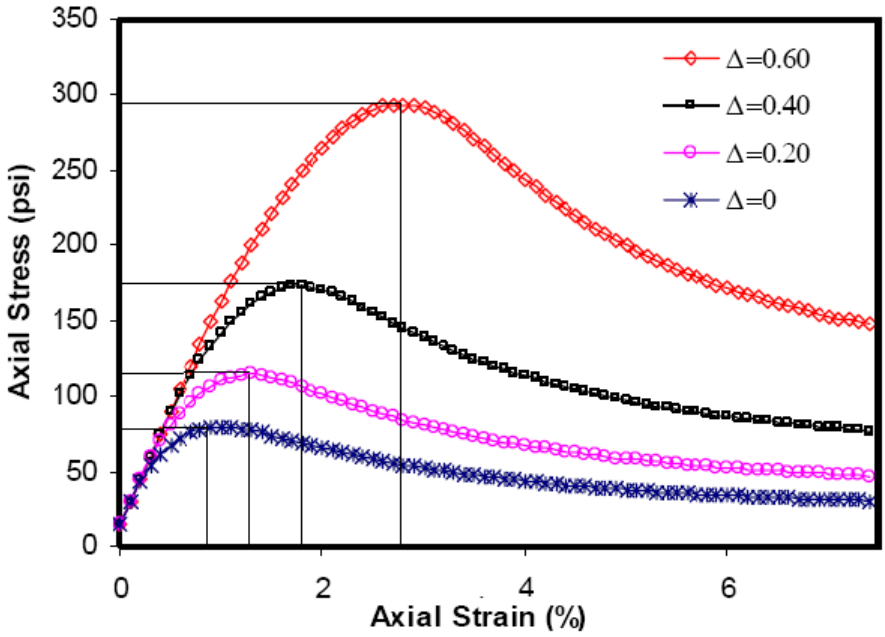

Figure 2.1: Influence of Anisotropy on Stress-Strain relationship [5].

Figure 2.1, shows within the same Vector magnitude, an increase in in axial strain results increase in axial stress. When anisotropy (Vector magnitude, Δ) increases the performance (stress-strain) of AC mixtures also increases. It deals, increasing anisotropy increases the percentage of particles oriented in the horizontal direction (i.e., leading to more contact and increase resistance to deformation in vertical direction). The anisotropic distribution of particles affect the relative sliding of particles and hence it influences the dilation of granular materials. The relationship between anisotropy and dilation has been studied experimentally by several researchers [19, 28].

2.2.2 Pavement Performance Tests

The performance of the AC is greatly influenced by the properties of the asphalt binding materials. The viscoelastic rheological properties of asphalt binders and mastics under an imposed shearing stress are time and temperature dependent and play a significant role in AC mechanical response.Characterization of the viscoelastic rheological properties of the asphalt binders and mastics were performed on a PG 76-22 unaged and an RTFO-aged binder and mastics produced with this binder using *Smartpave*® dynamic shear rheometer (DSR) at a single testing temprature of 60^oC [33].

Performance tests for Hot mix asphalt is conducted depending on Pavement distress type. Several studies shows that AC mixtures with similar density can exhibit very different response to loading. Accumulation of permanent deformation under traffic loading provide significantly different mechanical performances [2]. This observation indicates that density of AC mixtures is not a sufficient performance criterion and could be misleading in some cases.

2.3 Aggregate Properties

The physical properties of aggregates certainly have an important influence on the performance of AC pavements [15]. Aggregates used in the surface of the flexible pavement are subjected to wear under a heavy in-service traffic. Aggregates are subjected to crushing and abrasive wear during manufacturing, placing, and compacting AC. Therefore aggregates must be hard and tough enough to resist degradation and disintegration. The mineral composition and surface characteristics of aggregates also affect the bonding between aggregates and binder.

Aggregates of high quality have a strength of about 3.0 MPa and above, while the stress that highway pavement can experience is about 0.5 MPa, it can be concluded that most of the aggregates should be in the linear elastic range. Mechanical properties of aggregates are: modulus, E, Poisson's ratio, ν and strength. Intact rocks with distributed discontinuity are crushed into aggregates of different sizes; the porosity of aggregates becomes smaller and the modulus of aggregates are typically larger for aggregates of smaller size.

Rocks may be modeled as isotropic or anisotropic linear elasticity, viscoelasticity, plasticity, plasticity and viscoplasticity. These models affect the mixture properties especially anisotropy. For the same type of rock, porosity may vary. In addition, when particle sizes become smaller, the porosity typically decreases as well. For computing efficiency, aggregates may be considered as linear elastic and brittle with a stress-strain relationship as linear elastic-perfect plastic. While, aggregates are anisotropic, the random orientation effects and the material anisotropy may cancel out. Strengths of rocks are typically considered to follow Mohr-Coulomb criteria.

DIP allows easy access to aggregate morphological characteristics and leading to more precise and realistic parameters determination [11, 13, 14]. Morphological characteristics of aggregates are obtained through shape, angularity and texture properties [11, 14, 29]. Shape characteristics of aggregates represent flat and elongated particles, which are undesirable in the preparation of AC mixtures they break easily under loading effects. Angularity represents variations in the medium dimension superimposed on shape and can be measured through a parameter called roundness that ranges from 0 to 1 [32]. A value closer to 1 indicates circular object while 0 is line.

Texture represents variations in the small dimension super imposed on angularity. Local curvature of particles at the contact is important in load transfer among the skeleton, while the texture at the interface between aggregates and binder is important for durability. We need to separate the shape, angularity and texture. The physical properties of aggregate such as shape (form), angularity (roundness) and surface texture governs the rutting resistance of AC pavements. There are various image-based direct quantification methods for shape, angularity and texture (i.e., wavelet analysis). Figure 2.2, represents the aggregate geometry using three distinct physical properties, namely shape (form), angularity (roundness) and surface texture.

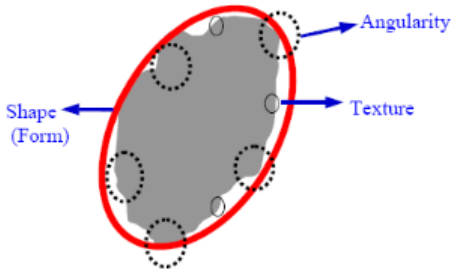

Figure 2.2: Components of Aggregate shape properties [14].

2.4 Methods for Measuring Internal Structure Distribution

Internal structure is typically referred to as microstructure in material science and fabrics in geomaterials. Internal structure of AC mixtures refers to the directional and spatial arrangement of the mixture constituents (aggregates, asphalt and air voids) as well as the chemical and physical interactions among these constituents [29]. Methods used to quantify the internal structure of AC mixtures can be divided in to two categories: volumetric analysis and imaging methods [13].

2.4.1 Volumetric Analysis Method

Volumetric analysis methods rely on bulk measurement of the percentage air voids in certain aggregate sizes or in the whole mixtures as indicators of packing [13]. It is currently used in *Superpave*® design system for dense-graded HMA, stone matrix asphalt design and Bailey method for selection of aggregate gradations in HMA. Recently, Volumetric analysis is implemented using DIP algorithm to process horizontally sliced AC X-ray CT images [36]. The algorithm is referred to as Volumetric based global minima (VGM) thresholding using *MATLAB*®.

VGM uses volumetric properties as the main criterion for establishing gray level threshold for the boundaries between air-mastic and mastic-aggregates by minimizing the error between the relative volume of the gray image and the corresponding property of the AC mixtures. For three phases, circular sections gives the air-mastic gray threshold is relatively insensitive to the air void content while, the mastic-aggregate gray threshold increases with decreasing aggregate volume. VGM produces realistic rendering of the microstructure of AC mixture and significantly improves images compared to raw X-ray CT images.

2.4.2 Imaging Method

The imaging method quantify the distribution of the aggregate skeleton, voids in mineral aggregate and air voids by analyzing images of the internal structure. It involves three major steps: image acquisition, processing and analysis. Images of the internal structure can be captured with a setup that consists of a microscope and a camera or 3D with an X-ray CT images. Several studies have demonstrated the potential application of X-ray CT technology to characterize different properties of AC mixtures [1, 12, 13, 15, 30, 32, 36, 37]. During acquisition of image different chemicals like hydrofluoric acid may use to discolor different types of rocks, especially those rich in iron such as diabase aggregate [23]. It is used to facilitate capturing quality images that allow separating aggregates from the other phases on the basis of differences in color. Image analysis techniques are applicable in knowing compaction and mechanical properties to measure aggregate orientation in specimens compacted to different number of gyrations and field cores [12, 13, 25].

2.5 Anisotropy of Granular Materials

Anisotropy of a material is the property of being directionally dependent [27]. The anisotropy of an AC mixture can be defined as difference in physical properties such as Modulus, E and Poisson's ratio, ν when the AC mixture is measured in different directions. AC mixtures was demonstrated to be cross anisotropic materials in both laboratory and field tests [27, 37]. Origin of anisotropy in granular materials such as soils, aggregate base and asphalt mixtures, consists two types of anisotropy: 1) inherent anisotropy and 2) stress-induced anisotropy [15, 37].

There are three sources of anisotropy: [1] the anisotropic distribution of contact normals, which is indicative of the mutual relation among particles; [2] preferred orientation of non spherical air voids; and [3] the preferred orientation of non spherical particles. Among the three sources of anisotropy, biaxial compression test on two dimensional assemblies was conducted and observed that inherent anisotropy by [1] and [2] tends to be completely altered during the relatively early stage of non-elastic deformation, while inherent anisotropy by [3] still remains at the later stage of deformation [20].

Inherent and stress induced anisotropy will first be interpreted in terms of particle alignment. In order to avoid the influence of the stress-induced anisotropy and to obtain pure inherent anisotropy, all AC mixture specimens are tested with small strains using both laboratory and field tests. Triaxial tests on cubic field samples are conducted and shows significant differences in vertical and horizontal stiffness [30]. They further analyzed the pavement responses in a finite element program by using anisotropic and isotropic moduli, separately. They found larger tensile and shear stresses in the pavement when using anisotropic moduli than when using the isotropic modulus.

In order to define quantitatively the inherent anisotropy of the particle orientation, originally the fabric tensor (F_{ij}) is given by Equation 2.1 [18, 20]:

$$F_{ij} = \int_{\Omega} m_i m_j E(m)\, d\Omega \qquad (i,j = 1,2,3; \Omega = 4\pi) \tag{2.1}$$

Where;

- F_{ij} = Fabric Tensor.
- Ω = a solid angle corresponding to the entire surface of a unit sphere;

- m_i and m_j (i, j = 1,2,3) = components of a unit vector m projected on the orthogonal reference axes x_i (1,2,3); and
- $E(m)$ = Probability density function that describes the spatial distribution of the vector m.

Fabric tensor is a symmetric second rank tensor which characterizes the geometric arrangement of the porous material microstructure. Fabric tensor for 3D assemblies of granular material is introduced as an index showing the anisotropy due to the preferred orientation of constitutive particles. It has three principal values corresponding to three principal directions (three principal axis of anisotropy).

The derivation relies two assumptions: [1] the inherent anisotropy exhibits axial symmetry with a symmetry axis parallel to the vertical direction, and [2] major and minor axes of the aggregate distribution corresponds to the horizontal and vertical directions, respectively [20]. Material symmetries of orthotropy, transverse isotropy and isotropy corresponds to the case of three, two and one distinct eigenvalues of the fabric tensor, respectively.
For transversely isotropic granular media, the $E(m)$ is neglected and the Fabric tensor (F_{ij}) is formulated as using Equation 2.2.

$$[F_{ij}] = \begin{bmatrix} F_1 & 0 & 0 \\ 0 & F_2 & 0 \\ 0 & 0 & F_3 \end{bmatrix} = \frac{1}{3+\Delta} \begin{bmatrix} 1-\Delta & 0 & 0 \\ 0 & 1+\Delta & 0 \\ 0 & 0 & 1+\Delta \end{bmatrix} \tag{2.2}$$

Where; Δ = Vector magnitude that is used to quantify the directional distribution of particles and is calculated by Equation 2.13.

The 2-D fabric tensor is transferred to a 3-D fabric tensor (F'_{ij}) as show in Equation 2.5 that has a similar form to the original 3-D fabric tensor shown in Equation 2.2 [15, 20]. The fabric tensor (F'_{ij}) can be employed when using continuum mechanics principles to study AC mixtures or granular bases using Equation 2.5.

$$[F'_{ij}] = \begin{bmatrix} F'_1 & 0 & 0 \\ 0 & F'_2 & 0 \\ 0 & 0 & F'_3 \end{bmatrix} = \frac{1}{3+\Delta'} \begin{bmatrix} 1-\Delta' & 0 & 0 \\ 0 & 1+\Delta' & 0 \\ 0 & 0 & 1+\Delta' \end{bmatrix} \tag{2.3}$$

Where; Δ' = Modified Vector magnitude that is used to quantify the directional distribution of particles and is calculated by Equation 2.15.

Recently, a relationship between the modified Vector magnitude (Δ') and modulus ratio (E^*_{11}/E^*_{22}) in order to quantify the inherent anisotropy of the AC mixtures was theoretically presented by [37]. Subsequently, he verify experimentally. The development of the relationship between modified Vector magnitude and modulus ratio starts from the general polynomial relation between the elastic modulus tensor and the fabric tensor of an elastic material [3, 26]. In the case of granular materials such as soils, aggregate base and AC mixtures, the high order terms in the polynomial function can be neglected and the elastic relation becomes [18, 20, 25]. Equation 2.4 shows elastic modulus tensor.

$$C_{ijkl} = 2b_6\delta_{ik}\delta_{jl} + 4b_7F'_{ik}\delta_{lj} \qquad i,j,k,l = 1,2,3 \tag{2.4}$$

Where;

- C_{ijkl} = Elastic modulus tensor
- δ_{ij} = Kronecker delta
- F'_{ik} = 3D fabric tensor given in Equation 2.5.
- b_6 and b_7 = Material constants which is given by Equation 2.5 [20].

$$\begin{cases} b_6 = \frac{1}{4} - \frac{\mu}{2}\sqrt{2D_2} \\ b_7 = \frac{3}{4}\mu\sqrt{2D_2} \end{cases} \tag{2.5}$$

Where; μ = experimentally determined parameter and D_2 = Second invariant of the deviatoric fabric tensor. The deviatoric fabric tensor can be calculated using Equation 2.6.

$$F_{ij}^{''} = F_{ij}^{'} - \frac{1}{3}F_{kk}^{'}\delta_{ij} = \frac{2\Delta^{'}}{3(3+\Delta^{'})}\begin{bmatrix} -2 & 0 & 0 \\ 0 & 1 & 0 \\ 0 & 0 & 1 \end{bmatrix} \tag{2.6}$$

The second invariant of the deviatoric fabric tensor (D_2) is determined using Equation 2.7.

$$D_2 = \frac{1}{2}F_{ij}^{''}F_{ji}^{''} = \frac{4\Delta'^2}{3(3+\Delta')^2} \tag{2.7}$$

After some derivation, an approximate linear relation between $\sqrt{D_2}$ and $\sqrt{E_{11}^*/E_{22}^*}$ is developed which is given in Equation 2.8 [37].

$$\sqrt{D_2} = \frac{2\sqrt{3}\Delta'}{3(3+\Delta')} = k\left(\sqrt{\frac{E_{11}^*}{E_{22}^*}} - 1\right) + b \tag{2.8}$$

Where; k and b are the slope and intercept of the fitting line, respectively. By applying the above relation to the AC mixtures and using the boundary condition as follows:

- If $\Delta' = 0$, then $\sqrt{D_2} = 0$, the aggregates are randomly distributed and the material is isotropic, which indicates $E_{11}^*/E_{22}^* = 1$.
- If $\Delta' = 1$, then $\sqrt{D_2} = \frac{1}{2\sqrt{3}}$, the aggregates orient along one direction, the material is fully cross anisotropic, and the modulus ratio E_{11}^*/E_{22}^* has the maximum value (let max. $E_{11}^*/E_{22}^* \equiv$ q).

Employing two boundary conditions in Equation 2.8 to solve for k & b yields:

$$\begin{cases} k = \frac{\sqrt{3}}{6(\sqrt{q}-1)} \\ b = 0 \end{cases} \tag{2.9}$$

Substituting Equation 2.9 into Equation 2.8, the relation between Δ' and E_{11}^*/E_{22}^* is developed as:

$$\Delta' = \frac{3\left(\sqrt{\frac{E_{11}^*}{E_{22}^*}} - 1\right)}{4(\sqrt{q}-1) - \left(\sqrt{\frac{E_{11}^*}{E*_{22}}} - 1\right)} \tag{2.10}$$

The above theoretical derivation is verified experimentally by [37]. The modulus ratio is measured having frequencies of the vertical and horizontal modulus ranges from 0.05Hz to 50Hz for each replicate of the mixture with the same asphalt binder, air void content and aging period. Using regression analysis, the modulus ratio (q) is to be 2.808 with an R-squared value 0.9439 [37]. The reasonable value of the maximum modulus ratio and the high R-squared value demonstrate the goodness of this model. Due to this the developed Equation 2.10, is applicable in nondestructive testing data.

$$\Delta' = \frac{3\left(\sqrt{\frac{E^*_{11}}{E^*_{22}}} - 1\right)}{2.703 - \left(\sqrt{\frac{E^*_{11}}{E*_{22}}} - 1\right)} \qquad R^2 = 0.9439 \tag{2.11}$$

In addition, Regression analysis is also performed on original vector magnitude (Δ), which indicates that the maximum modulus ratio (q) is 10.9 that is impossible for an AC mixtures and the R-squared value is only 0.4559. It indicates that inclination angle of the aggregate alone is insufficient to appropriately quantify the inherent anisotropy of the AC mixtures and the original vector magnitude is not applicable for granular media having a non-uniform distribution of particle size and shape.

$$\Delta = \frac{3\left(\sqrt{\frac{E^*_{11}}{E^*_{22}}} - 1\right)}{9.206 - \left(\sqrt{\frac{E^*_{11}}{E*_{22}}} - 1\right)} \qquad R^2 = 0.4559 \tag{2.12}$$

The next chapter discuss on analysis of aggregate orientation and the results of modified vector magnitude for characterizing inherent anisotropy of AC mixtures.

2.5.1 *MATLAB*® Software

The name MATLAB stands for MATrix LABratory. It is a high performance language for technical computing [16]. It integrates computation, visualization and programming environment. It has sophisticated data structure, contains built in editing and debugging tools like image processing toolbox, graphics capabilities and supports object oriented programming. To date, different commercial image analysis software were developed, however *MATLAB*® preferable over others. Because, have direct access to any portion of the image, it is possible to stop any calculation at any time, change a portion of the calculation procedure, restart the calculations from the point which was affected or from the beginning. Due to these, *MATLAB*® is an excellent tool for research. Image processing toolbox is a collection of functions that extend the capabilities of the MATLAB's numeric computing.

2.6 Aggregate Orientation

Approximately, 85% of the total volume of AC mixtures is consists of aggregates. It is not surprising that, the performance of AC mixtures is influenced by the properties of aggregate blends, such as grading, shape (angularity and elongation) and texture (roughness). The characteristics of aggregate including shape and orientation have a great influence on the inherent anisotropy of AC mixtures. The orientation of the aggregates was measured by the angle between its major axis and a horizontal line on the scanned image. The major axis length is defined by the greatest distance between two pixels of the boundary contour. The minor axis of an aggregate cross section is defined as the longest line that can be drawn perpendicular to the major axis.

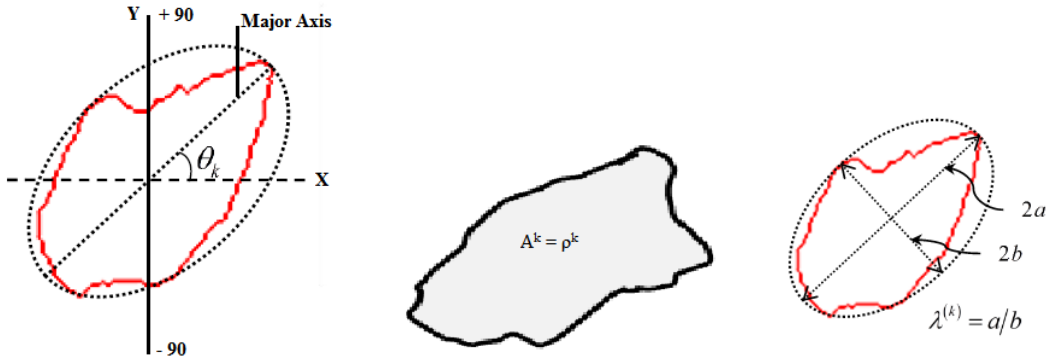

Figure 2.3: Measurement of k-th Aggregate characterstics (a) inclination angle (b) surface area and (c) Aspect ratio [37].

2.7 Vector Magnitude

Vector magnitude is defined as an internal microstructural index which is used to quantify the average inherent anisotropy of AC mixtures. Preferential orientation of geologic structures, a parameter of Δ and average angle of inclination from the horizontal was first introduced for quantification of two dimensional orientation of data [4]. Subsequently, the inherent anisotropy of soils in terms of the inclination of soil particles by using the concept of Vector magnitude which was then used to formulate the microstructure-based fabric tensor to modify the effective stress in the soils during continuum damage analysis [18, 20]. Equation 2.13, shows Vector magnitude for AC mixtures.

$$\Delta = \frac{1}{M}\sqrt{\left(\sum_{k=1}^{M} sin2\theta_k\right)^2 + \left(\sum_{k=1}^{M} cos2\theta_k\right)^2} \tag{2.13}$$

$$\theta = \frac{\sum_{k=1}^{M} |\theta_k|}{M} \tag{2.14}$$

Where;

- Δ = Vector Magnitude.
- M = Total number of aggregate particles analyzed on an image.
- θ_k = is the inclination angle of the major axis of the k^{th} aggregate particle measured from the horizontal axis in the image.
- θ = Average angle of inclination from the horizontal.

Vector magnitude (Δ) was used to quantify the directional distribution of coarse aggregates [13, 15, 23, 25]. The number (k=1,2,3,...M) and inclination angle θ_k of the coarse aggregate were obtained by photographing the cut surface or scanning the AC mixture using the X-Ray CT images.

Formulation of fabric tensor and vector magnitude shown in Equation 2.2 and 2.13 are designated for fine grained materials with approximately uniform particle size, such as soils. Theses formulations may not be directly applied to aggregates in an AC mixture which don't have uniform particle size or uniform shape.

However, the vector magnitude and fabric tensor should be modified so it can address not only the inclination of coarse aggregates but also the size, orientation and sphericity of both coarse and fine aggregates [37]. The modification of the fabric tensor and the vector magnitude are as follows [37];

$$\Delta' = \frac{1}{A_o}\sqrt{\left(\sum_{k=1}^{M} \rho^{k}\lambda^{k} sin2\theta_k\right)^2 + \left(\sum_{k=1}^{M} \rho^{k}\lambda^{k} cos2\theta_k\right)^2} \tag{2.15}$$

Where;

- Δ' = Modified Vector Magnitude.
- ρ^{k} = area of k^{th} aggregate on the image of the asphalt mixture.
- λ^{k} = sphericity or aspect ratio of k^{th} aggregate.
- $A_o = \sum_{k=1}^{M} \rho^{k}\lambda^{k}$

As we see from Equation 2.4, the modified vector magnitude addresses the effects of the aggregate size, orientation and sphericity of both coarse and fine aggregates on the inherent anisotropy. By comparing Equation 2.13 and Equation 2.15, modified vector magnitude can be interpreted as follows [37]. The effect of the inclination angle on the anisotropy of an AC mixture is emphasized or de-emphasized based on the aggregate size (area) and sphericity (aspect ratio). For example, if the aggregate is larger or more flat and elongated, the inclination angle will contribute more anisotropy to the mixture. If the aggregate is smaller or has a more rounded shape, the net effect is to decrease the influence of the inclination angle on anisotropy.

Chapter 3

Research Methodology

3.1 Materials

In chapter 1 and 2, background of the study, statement of the problem and the most relevant literature on addressing analysis of aggregate orientation with inherent anisotropy in AC mixtures were described. In this study, we use secondary data's especially, for the experimental work (i.e., X-ray CT images) taken from [33]. Aggregates transmit the wheel loads through internal friction and interlocking. Coarse and fine aggregates are considered in this study. Sources of aggregate are taken from three Texas DOT districts. Different Experimental tests are performed on aggregates. Among them, gradation test were considered for this study. Aggregate gradation tests were performed using Tex 401-A specifications on dried aggregates to obtain the percentage of fines passing sieve No. 200 using Texas DOT method.

Air voids attained within AC mixtures for this study is from 3-4%. Asphalt mastics are blends of asphalt binder and mineral fillers passing sieve No. 200. Each of these mixture designs was prepared with a PG 76-22 modified binder meeting the Texas DOT specifications with AASHTO T240/ASTM D2872 procedures using a *SmartPave*® dynamic shear rheometer (DSR) apparatus at a single testing temperature of 60^oC. The asphalt binder was supplied by the Valero Ardmore Refinery in Oklahoma, United States.

AC mixtures were prepared using Tex-241-F and Tex-205-F specifications. There are three AC mixture designs: Coarse Matrix High Binder Type C (CMHB), Porous Friction Course (PFC) and Superpave Type C (Superpave) AC mixtures.These mixtures were selected by Texas DOT. These AC mixtures were compacted using the Superpave Gyratory Compactor (SGC). The compaction process included a 600 kPa ram pressure, 1.25° gyration angle and 30 gyrations per minute. CMHB-C AC mixture is coarse graded composed of 63% coarse aggregate and 37% fine aggregate.

The PFC is a coarse, gap graded mixture with high percentage by weight of coarse aggregates. It is composed of 89% aggregates larger than a sieve No. 8. Superpave Type C is a fine-graded mixture consisting of 35% coarse aggregates and 65% fine aggregates. The properties of the aggregate and asphalt used for each mixture design are presented in Table 3.1 and the aggregate gradation curve is shown in Figure 3.1.

Table 3.1: Asphalt Concrete Mix Design Data [33].

Parameter	CMHB	PFC	Superpave
Binder grade	PG 76-22		
$P_b(\%)$	4.2	5.1	4.0
$V_a(\%)$	7.3	19.5	7.4
VMA(%)	12.7	27.2	12.7
VFA(%)	70.2	26.4	68.5
Sieve opening or Size (mm)	Percent Passing (%)		
1 in. (25)	100	100	100
3/4 in. (19)	99	100	99
1/2 in. (12.5)	78.5	90	95
No. 1/2 (9.5)	60	47.5	92.5
No. 4 (4.75)	37.5	10.5	77.5
No. 8 (2.36)	22	5.5	43
No. 16 (1.18)	16	5	30
No. 30 (0.6)	-	4.5	-
No. 50 (0.3)	-	3.5	-
No. 200 (0.075)	7	2.5	6

Where; P_b is Percent binder Content, V_a is Percent air Voids, VMA is Percent voids in mineral aggregates, and VFA is Percent Voids filled with asphalt.

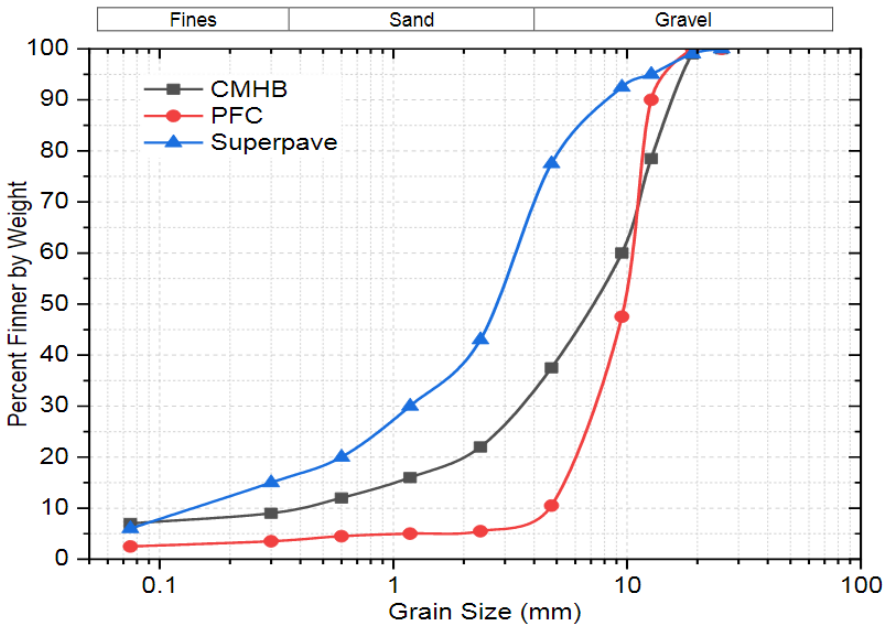

Figure 3.1: Aggregate Gradation curve for CMHB, PFC and Superpave AC mixtures [33].

3.2 Methods

The method that is going to be adopted in this research paper so as to analyze aggregate orientation and evaluates inherent anisotropic microstructure properties of AC mixture is an aggregate related geometric parameter, the modified vector magnitude using X-ray computed tomography (CT) images. It involves inherent anisotropic characterization of AC mixtures through modified vector magnitude, relationship between modified vector magnitude and physical properties. The methodology to be followed in carrying out these study is shown in Figure 3.5. Finally, Conclusion and Recommendations for future research study is given.

3.2.1 Volumetric Analysis

Volumetric analysis methods rely on bulk measurement of the percentage of air voids in certain aggregate sizes or in the whole mixture was discussed by [33]. The author discuss on loose and compacted mixtures, air void, binder content, VFA and specific gravity of AC mixtures. DIP algorithm is utilized to process horizontally sliced AC X-ray CT images using Volumetric based global minima (VGM) thresholding algorithm [36]. VGM produces realistic rendering of the of AC microstructure and significantly improves images compared to raw X-ray CT images.

3.2.2 X-Ray CT Scanning

X-ray CT imaging is a powerful non-destructive technology for acquiring 3D microstructure of heterogeneous materials (i.e., AC mixtures) took place at Texas A & M University. Each of three AC mixtures (150mm diameter by 165mm hight was cored and sawn to a diameter of 100mm and height of 150mm), respectively. Each image was scanned perpendicular to its axis at 1 mm distance interval to yield 148 slices per individual AC mixtures, ignoring the top and bottom slices. Each image have a raw format having 512 x 512 pixels. The resolution is 195µm per pixel, which doesn't allow detecting particles larger than roughly particles passing sieve No. 70. Capturing the AC microstructure through x-ray CT involves three major steps (image acquisition, processing and analysis). Components of X-ray CT images are shown in Figure 3.2. Figure 3.3, shows sample scanned vertical slice images.

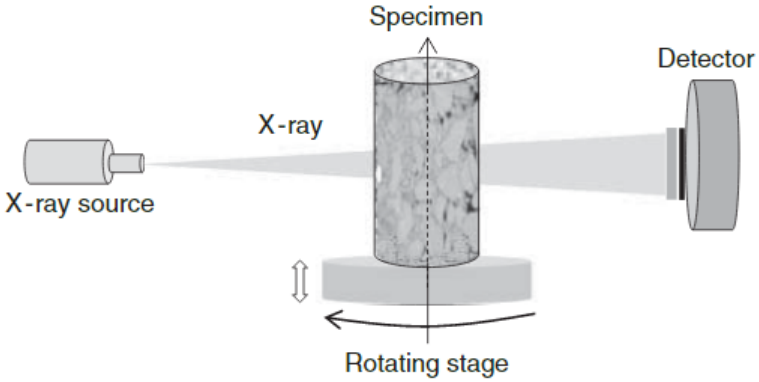

Figure 3.2: Componenets of X-ray CT system [33].

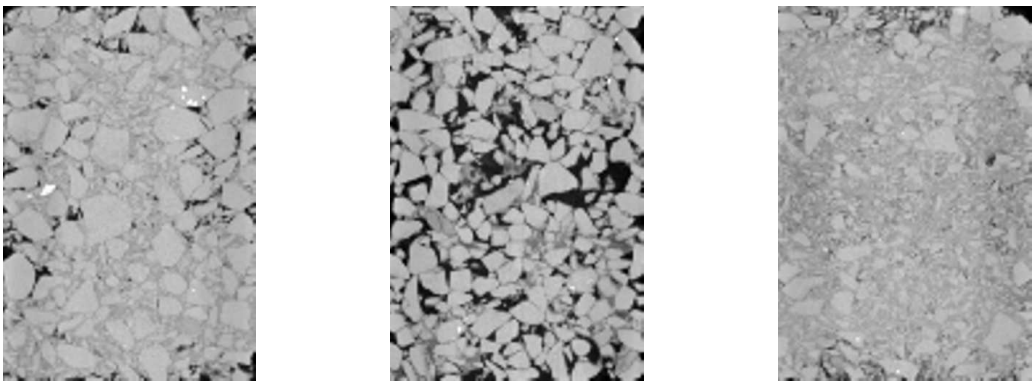

(a) (b) (c)

Figure 3.3: Typical Scanned Vertical slice Images: a) CMHB b) PFC and c) Superpave.

3.2.3 *MATLAB*®

To analyze aggregate orientation and evaluate inherent anisotropy of AC mixtures using microstructural parameter programs are written using *MATLAB*®, Image Processing toolbox for the given X-ray CT images. The method use image processing toolbox, specifically *regionprops* and *bwboundaries*. Basically, MATLAB codes are developed to process and analyze X-ray CT images. An Automated image processing algorithm was developed, using Adaptive Enhanced based Thresholding Algorithm (AETA) to process the scanned images and effectively separate connected or overlapping coarse and fine aggregate sizes ranging from 1.18mm to 19mm. Adaptive thresholding depends on local histogram or gray level information (histogram of image is uniform) for three AC mixtures.

Typical scanned images are processed and analyzed using *MATLAB*® software. Processing of images are done to remove poor contrast and remove noise for the scanned images. It includes image Enhancement, noise removal, Edge Detection, image segmentation and Thresholding. The output in image processing are pictures. Image analysis is different from processing of images. Because the outputs are numerical rather than a pictures. Basic commands to analyze images are *regionprops* and *bwboundaries*. Morphological characteristics of aggregates (i.e., orientation, Area, major axis, minor axis and perimeter) are obtained from image analysis.

3.3 Statistical Analysis

Using the measured data of an aggregate morphological properties; statistical parameters can be used to represent the entire distribution of AC microstructure. The objective of this analysis was to determine variability in different aggregates on the basis of image analysis results between and within AC layers whether or not all the means are equal. Some of the statistical parameters for horizontal slice are: orientation, vector and modified vector magnitude values for top, middle and bottom layers within different mixtures.

Selection of sample size for AC layers i.e. top, middle and bottom layers is arbitrary. Scheffe pair wise multiple comparison tests can used determine which means differ within these groups. For our test, we have 148 experimental units (i.e., slice images), dependent variable is orientation and AC layers are factor variables.

The statistical analysis is done using STATA V14.0 software. ANOVA was done to study the variability in image analysis results. Figure 3.4, shows statistical analysis sample size determination for horizontal slice AC mixtures.

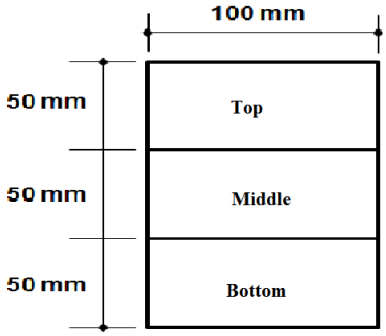

Figure 3.4: Sample size determination for Horizontal layer AC mixtures.

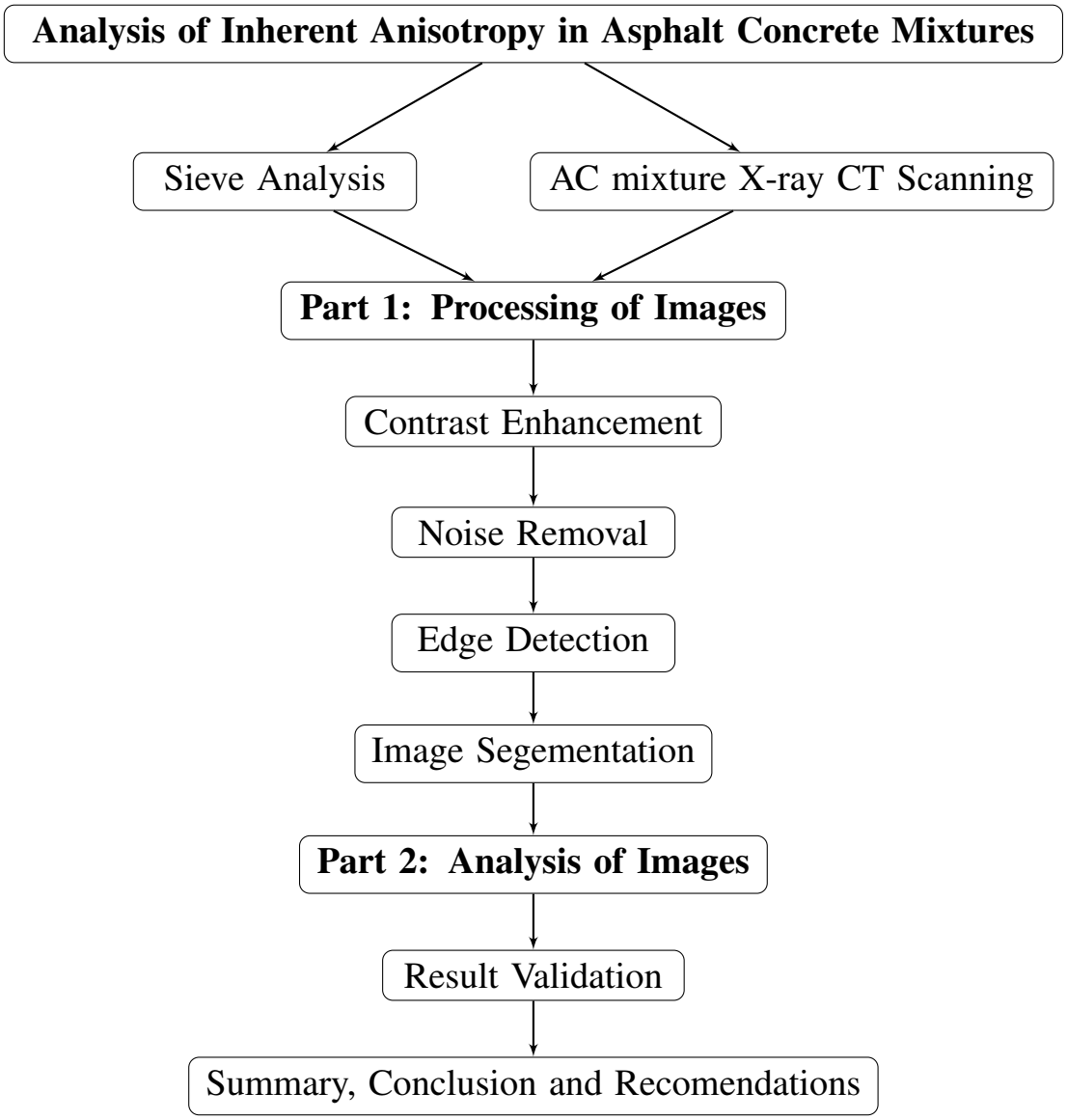

Figure 3.5: Research Methodology Flow Chart.

Chapter 4

Results and Discussion

4.1 Digital Image Processing

Asphalt Concrete has been recognized as anisotropic material in both laboratory and field tests [37]. However, the degree of anisotropy and its implications in pavement design and analysis have not been well understood. This paper analyze aggregate orientation and evaluate inherent anisotropy of AC mixtures through vector and modified vector magnitude. Image processing is used in various applications such as material science, remote sensing, medical imaging, military, film industry, document industry, graphic arts [6]. There are two methods in image processing: Analog and Digital image processing. Among the two DIP was considered for this study.

Digital Image Processing is the term that pertains to converting video images into a digital form and applying various mathematical procedures to extract significant informations from the picture. It has been applied to the quantitative investigation of coarse aggregate orientation in AC mixtures by examining statistically the differences between the aggregate particles on horizontal and vertical cross sections of the AC mixtures. Advantages of DIP method is its versatility, repeatability and preservation of original data precision. DIP algorithm involves three stages. MATLAB codes for three AC mixtures are given on Appendix A and Appendix B.

4.1.1 Processing of Images

Asphalt Concrete X-ray CT images consists of pixel representations that vary in gray scale level between 0 (i.e., black) and 1 or 255 (i.e., white). Raw X-ray CT images have poor contrast and include a variety of type of noise. Figure 4.1 illustrates processed 2D rectangular AC sliced mixtures having noise, poor contrast.

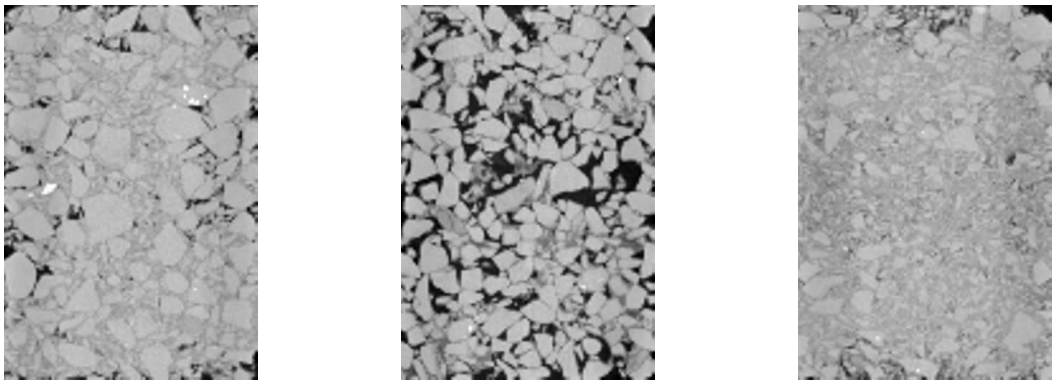

(a) (b) (c)

Figure 4.1: Input vertical slice AC mixtures: (a) CMHB (b) PFC and (c) Superpave.

Image Enhancement

Image contrast can be improved using different techniques: spatial domain (directly on pixels); histogram equalization and frequency domain (based on Fourier transform). Most commonly used method called histogram equalization using *MATLAB*® built in function *histeq* is implemented for this study to increase the quality of raw image [6]. It consists of adjusting linearly the gray level intensity of pixels to produce a more even distribution throughout the image. Figure 4.2 shows the gray level intensity in the abscissa and the number of pixels by gray-level in the ordinate for three 2D AC mixtures.

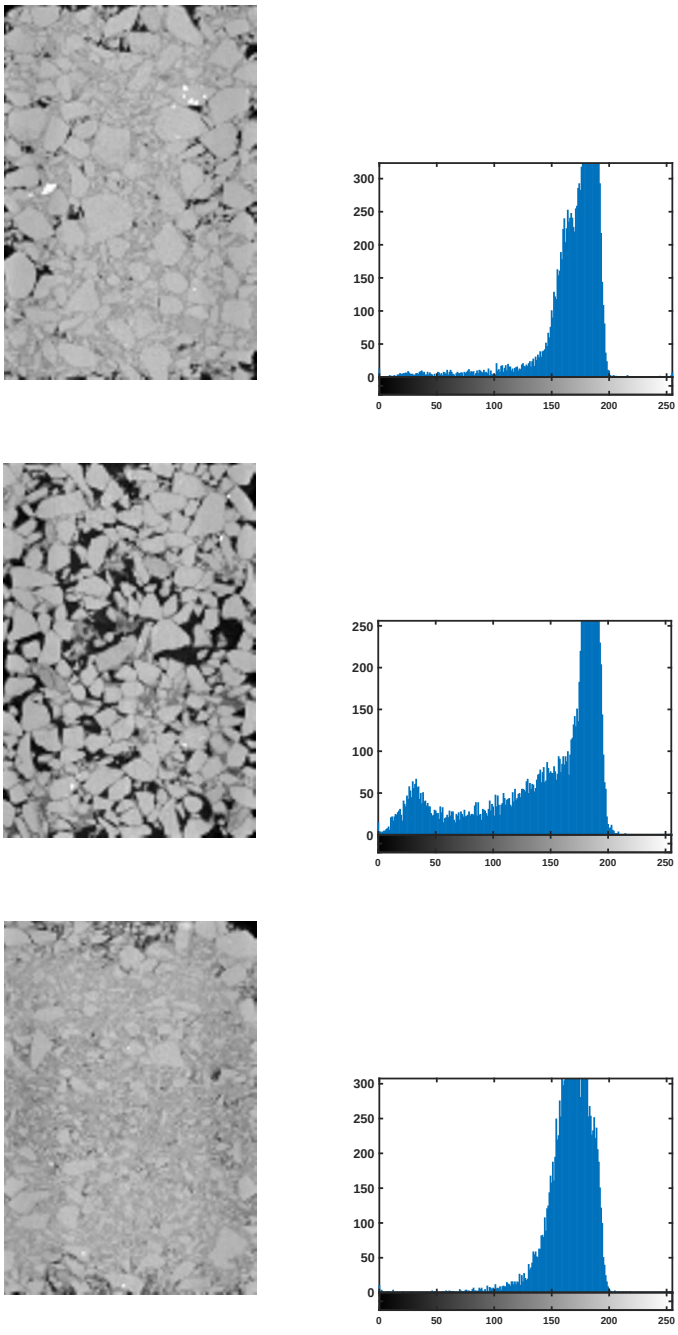

Figure 4.2: Processed AC mixtures with their Histogram: (a) CMHB (b) PFC and (c) Superpave.

Figure 4.3, shows the gray level intensity in the abscissa and the number of pixels by gray-level in the ordinate for histogram equalized three 2D AC mixtures.

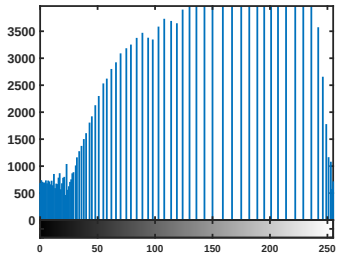

(a)

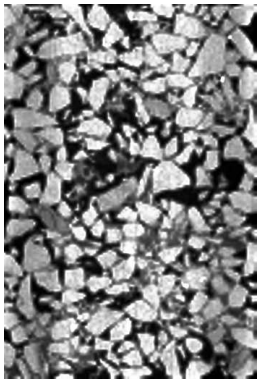

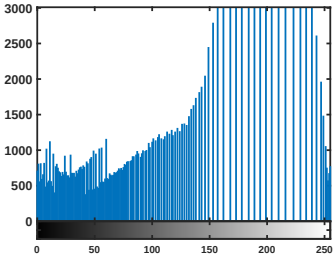

(b)

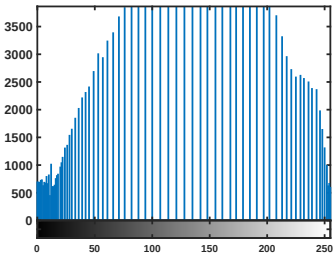

(c)

Figure 4.3: Histogram Equalized AC mixtures with their Histogram: (a) CMHB (b) PFC and (c) Superpave.

Noise Removal

X-ray CT images includes different types of noise. Its main sources are sensor quality, variations in densities within the individual mastic, aggregate, image digitizing and processing. Depending on the noise type two methods are commonly used for de-noising; median and mean filtering [6]. Median filtering, the gray level of each pixel is replaced by the median of the gray level of all pixel values in the pixel's neighborhood. While, mean filtering, the gray level of each pixel is replaced by the average of the gray level of all pixels neighborhood. In AC image de-noising, the median filtering technique has been used by several researchers [1, 15, 32]. Figure 4.4 shows, salt and pepper noisy 2D AC images. Figure 4.5 shows median filtered for 2D AC image using 3 x 3 kernel (local neighborhood in windows pixels in size).

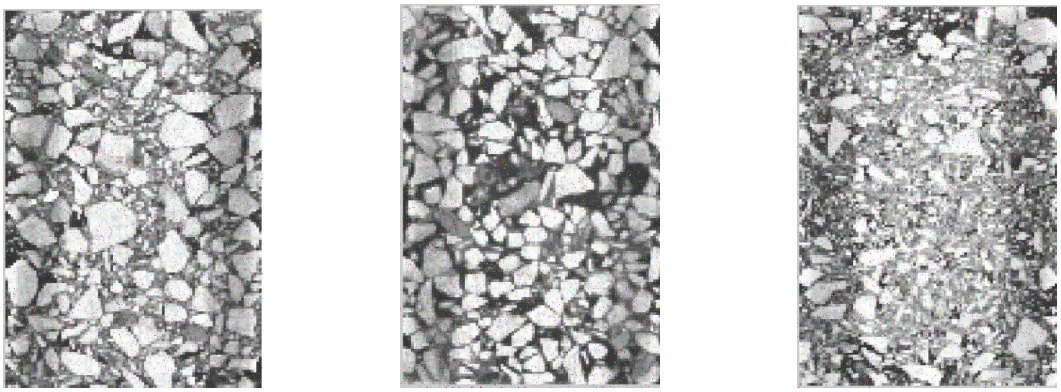

(a) (b) (c)

Figure 4.4: Salt & Pepper Noisy AC mixtures: (a) CMHB (b) PFC and (c) Superpave.

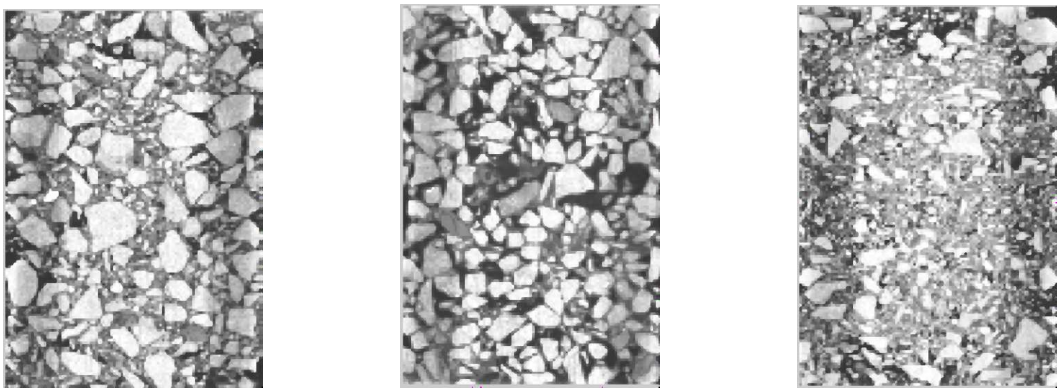

(a) (b) (c)

Figure 4.5: Median Filtered AC mix.: (a) CMHB (b) PFC and (c) Superpave.

Edge Detection

Processing is carried out through edge detection and Thresholding. Edge detection can enhance the physical boundaries between the three phases in AC. It is typically carried out using gradient approach. The gradient of an image is the magnitude of the 1st derivative of its image function (i.e., gray level $f(i, j)$) [6]. The direction of the gradient vector (i.e., the orientation of a unit normal vector perpendicular to the specified edge location) can also be used to quantify the orientation of the sharpest gray level intensity change.

$$\nabla f = \begin{bmatrix} G_x \\ G_y \end{bmatrix} = \begin{bmatrix} \frac{\partial f}{\partial x} \\ \frac{\partial f}{\partial y} \end{bmatrix} \tag{4.1}$$

Where; G_x and G_y denotes the partial derivatives in the x- axis and y-axis, the magnitude of this vector can be denoted by ∇f [6].

$$\nabla f = mag(\nabla f) = \sqrt{G_x^2 + G_y^2} \tag{4.2}$$

Where; ∇f indicates the maximum rate of increase of f(x,y) per unit distance in the direction of ∇f. In order to save computational source, in practice ∇f expression is usually simplified as the gradient vector [6].

$$\nabla f = \mid G_x \mid + \mid G_y \mid \tag{4.3}$$

The gradient image of the segmented regions of AC sample is implemented with $MATLAB^{®}$ programming and the coordinates of edges of aggregate are obtained. The abrupt changes in gray level intensity suggest phase boundaries. Sobel operator is not directly applicable in detecting boundaries between objects of different phases. Canny operator method is applicable in detecting boundaries between objects of different phases [9]. Figure 4.6 shows Canny Edge Detection for AC 2D mixtures for the boundaries of mastic phase and aggregate phase.

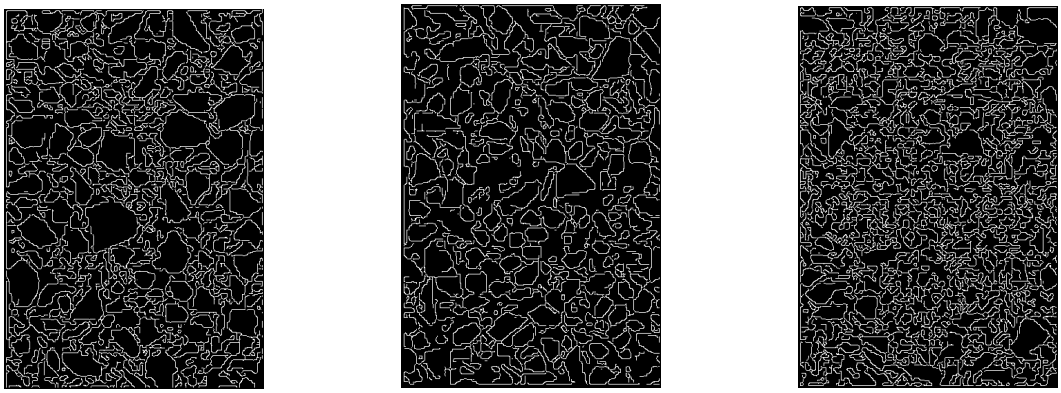

(a) (b) (c)

Figure 4.6: Canny Edge Detection of AC mixtures: (a) CMHB (b) PFC and (c) Superpave.

Image Segmentation

Quantifying the aggregates morphology and physical properties (i.e., shape, size, angularity, texture, orientation, segregation and contact zones) remains a difficult image processing task. Segmentation in the context of AC microstructure characterization is defined as the process of isolating aggregate particle from air voids and asphalt mastics. Image segmentation techniques play an important role in preserving the true aggregate structure in X-ray CT images. Segmentation can be generally classified in to four major categories: adaptive threshold, edge based, region based and watershed segmentation [6]. The most commonly used segmentation technique especially in civil engineering material application is watershed segmentation [10].

In this research, watershed image segmentation technique is utilized to effectively separate the overlapping (touching) mastic and aggregate objects using shape, color and texture features. It was performed using morphological dilation and erosion operations in *MATLAB*® [6]. The non-overlapping mastic and aggregate particles should be inputed to numerically analyze the different behavior of AC mixtures. Several researchers use numerical simulation technique called Discrete Element Method (DEM) to simulate permanent deformation behavior of AC. In this research numerical analysis technique called *MATLAB*® is used to analyze inherent anisotropy in AC mixtures. Figure 4.7 shows final segmented i.e non overlapped mastic and aggregate particles for 2D AC mixtures.

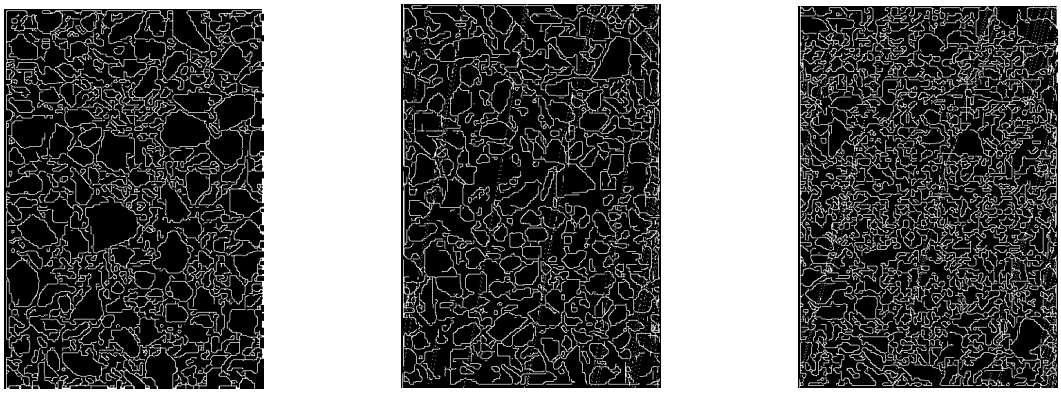

(a) (b) (c)

Figure 4.7: Final Segemented AC mixtures: (a) CMHB (b) PFC and (c) Superpave.

Thresholding

Thresholding is not only applicable in image processing. In any field threshold has the same meaning. It is simplest method of image segmentation. It is used to create binary images from grayscale image. There are different methods: Otsu's, global and adaptive method. Otsu's or automatic method is best when a good background to foreground contrast ratio exists. while, others are the most commonly used methods for identifying different phases in images of composite materials (i.e., AC mixtures).

Global thresholding is the simplest of all thresholding by taking histogram or gray level of complete image is partitioned by a single threshold T. Indeed, Adaptive Enhanced Thresholding Algorithm (AETA) or Local thresholding depends on local histogram or gray level information (histogram of image is uniform) for three AC mixture are shown in Figure 4.2. Global and adaptive thresholding techniques are employed by several researchers [10, 34, 36]. This methods depends on entirely on how well the histogram can be partitioned. If gray level is less than T it is labeled black (0) else it is labeled white (255). Regarding from the inspection of histogram for three AC mixture, we use Adaptive Thresholding algorithm we can find the value of T automatically.

1. Select initial estimate of T from the histogram.
2. Segment the image using T, this will produce a group of pixels having below or equal to T (G1) and greater than T (G2).

3. Compute the average gray level values μ_1 and μ_2 for pixels in region G1 and G2. μ_1 = count no. of pixels in G1/ T and μ_2 = count no. of pixels in G2/ T.
4. Compute new threshold using $T1 = 0.5(\mu_1 + \mu_1)$.
5. Repeat step 2-4 until the difference in T for successive iteration until smaller T get than the predefined parameter.

To separate the AC mixture phases, thresholding values (i.e., gray level) depends on mainly the Volumetric properties of AC mixtures (i.e., air, mastic and aggregate phases) which is presented by [33] using Volumetric Thresholding algorithm (VGA). Additional pixel processing is required to adjust the relative proportions of aggregate and mastic to reflect the actual volumetrics of the AC mixtures.

Figure 4.8, shows 2D rectangular sections after processing AC using Adaptive Thresholding for aggregate phases. It shows on white objects (grayscale = 255) represents aggregates while black objects (grayscale = 0) represents on non-aggregates. The images doesn't preserve the volumetric properties of the mixtures, as done by the VTA technique [22]. In addition, VTA produces a better separation between aggregates. A visual comparisons of images suggests that improvements in clarity between the pre-processed images and the thresholded images as shown above. In addition, the processed images show aggregates with more naturally-shaped edges. After thresholding a given image, image analysis of orientation and inherent anisotropy of the AC mixtures.

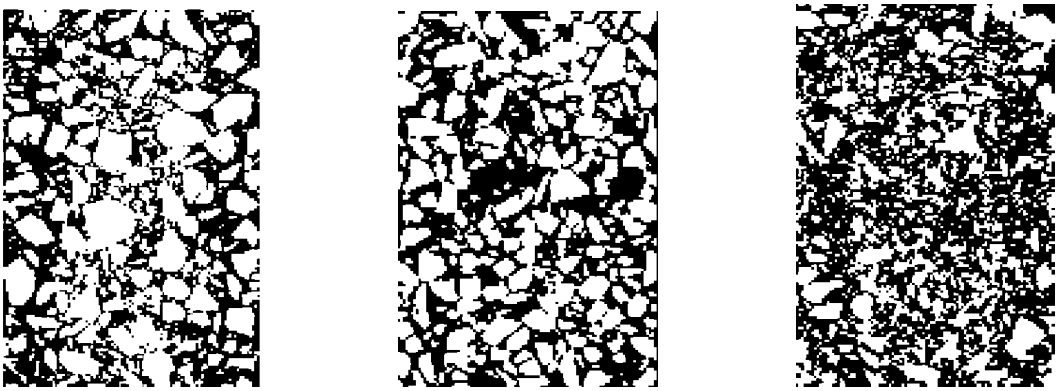

(a) (b) (c)

Figure 4.8: Adaptive Threshold AC mixtures: (a) CMHB (b) PFC and (c) Superpave.

4.1.2 Analysis of Images

Image analysis is different from other methods because image analysis procedures is a numerical output rather than a picture. MATLAB, image processing toolbox, *regionprops* tool automatically measure and gives the following aggregate morphological characteristics .

- Major axis: of the aggregate cross section is defined by the greatest distance between two pixels of the boundary contour.
- Minor axis: of an aggregate cross section is defined as the longest line that can be drawn perpendicular to the major axis.
- Perimeter: summation of all pixels forming the boundary of an aggregate cross section.
- Area: summation of all pixels contained within an aggregate cross section.
- Orientation: the angle between the major axis and the horizontal line (i.e., the x-axis) on the scanned image.

For three AC mixtures: the aggregate morphological properties for superpave Type C is smaller than the other AC mixtures. Because, there is greater concentration of fine aggregates are occurred than the others. For more, sample aggregate morphological characteristics of the horizontal slice No. 8 for three AC mixtures are given on Appendix C.

Aggregate Orientation

Image analysis were performed on each of the AC mixture specimens.The absolute values of the measured aggregate inclination angles ($|\theta_k|$) are classified in to 9 intervals: [0-10], [10-20], [20-30], [30-40], [40-50], [50-60], [60-70], [70-80], and [80-90]. Then the percentage of the aggregates in each interval is calculated using the number of aggregates in the corresponding interval divided by the total number of aggregates measured on the lateral surface of the specimen. Figure 4.9, shows distribution of aggregate orientation with their frequency of aggregates for CMHB Type C, PFC and Superpave Type C AC mixtures, respectively. In addition, Figure 4.10, shows summary on distribution of aggregate orientation with their frequency of aggregates for three AC mixtures.

Figure 4.9 and 4.10, shows that the average of approximately 20% of the aggregates has an inclination angle between -10^o-10^o and 65% of the aggregates have an inclination between -45^o - 45^o. This finding agrees with past studies [37]. Since a small inclination angle indicates the aggregates lies flat in the horizontal direction, the measurements demonstrate that the aggregates have a preferential distribution in the horizontal direction that is perpendicular to the compaction direction.

For three AC mixtures, the percentage of aggregates from -40^o - 50^o are comparably similar for CMHB and Superpave than PFC AC mixtures. In addition, percentage of aggregates decreases as aggregate orientation increases up to -40^o - 50^o for CMHB and Superpave Type C AC mixtures. It indicates, the percentage fine aggregates in two AC mixtures significantly influence the orientation of aggregate by aggregate-aggregate contact. In contrast, for PFC AC mixtures aggregate orientation nearly similar. Because, there is high amount of gap graded aggregates than fine aggregates.

Showing Standard Deviation is good to indicate the variability of the values, only when the distribution of the values is approximately normal (otherwise graphical representation of Standard Deviations are misinterpreted). We visualize the mean differences (between groups) rather than data differences. Due to this, differences between groups are plot together with their 95% confidence intervals. The error bars show variations of Standard Deviation ($\pm$) to an observed mean.

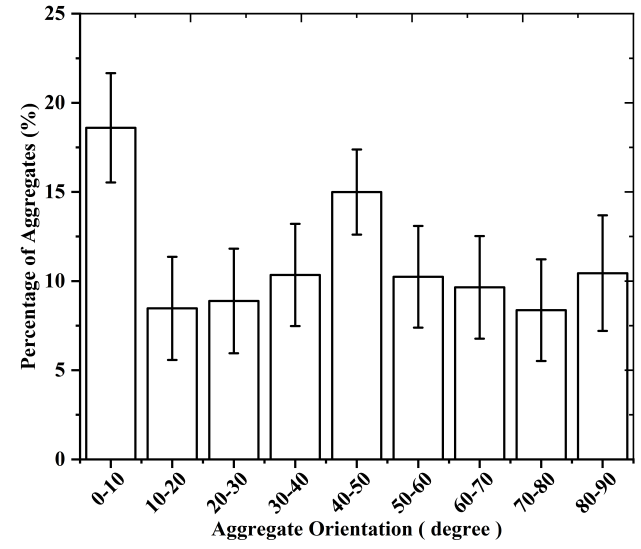

(a)

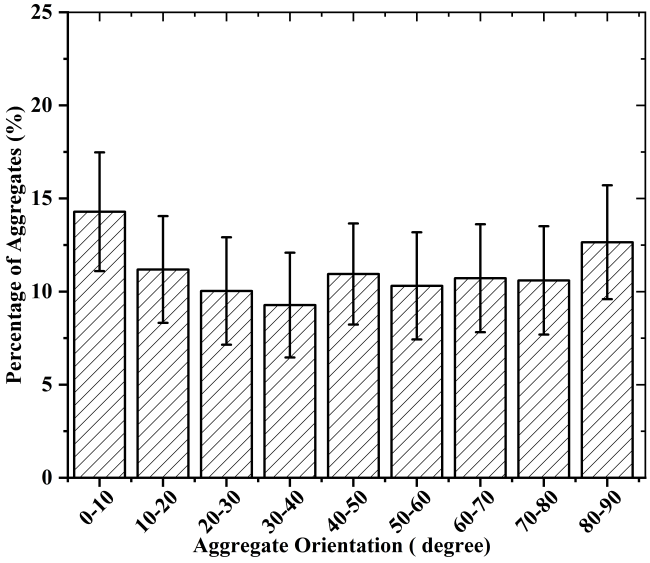

(b)

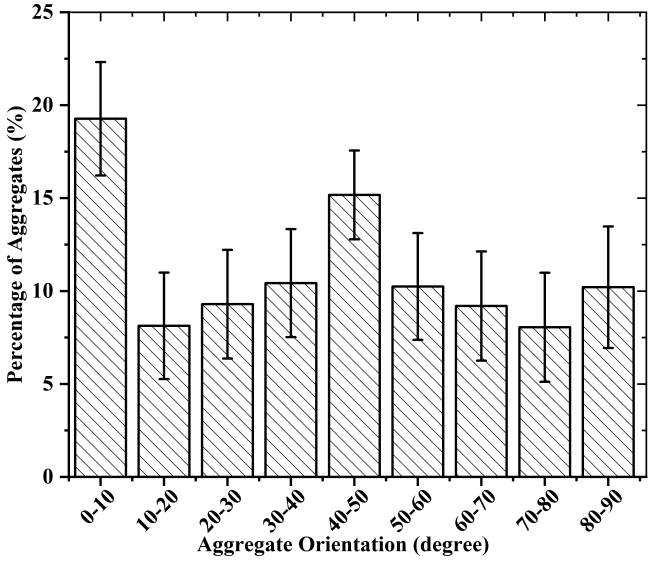

(c)

Figure 4.9: Distribution of Aggregate Oritentation: (a) CMHB (b) PFC and (c) Superpave.

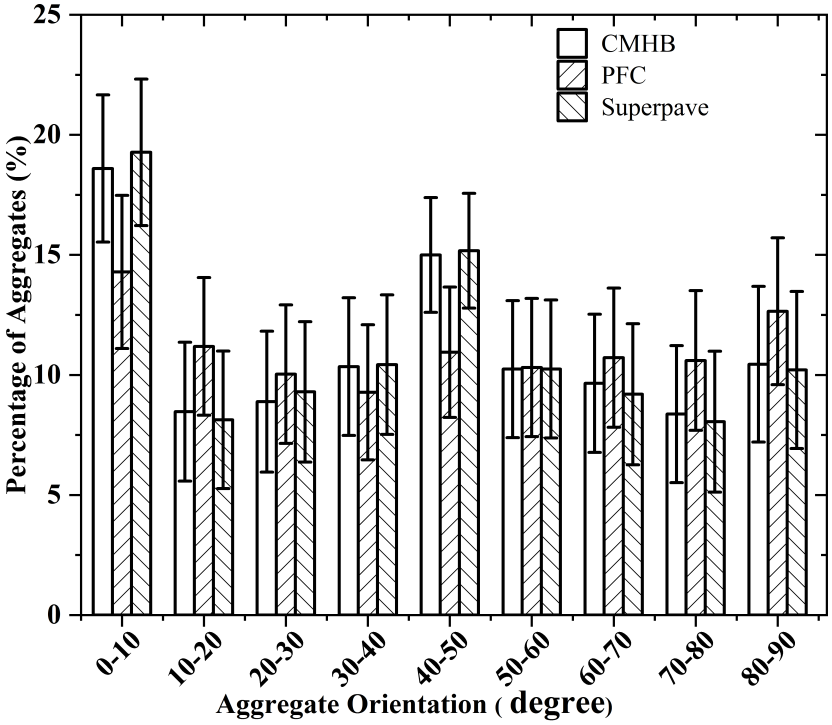

Figure 4.10: Distribution of Aggregate Orientation.

Vector Magnitude

The Vector (Δ) and modified Vector magnitude ($\Delta^{'}$) index, given in Equation 2.13 and 2.15 respectively, can be used to capture the directional distribution of the aggregate particles and in turn to evaluate the inherent anisotropy of AC mixtures. As stated earlier, the value of Δ ranges between 0 and 1, inclusively. A smaller vector magnitude indicates that the aggregate particles are more randomly distributed while a larger value of the vector magnitude indicates that the aggregate particles are oriented in one direction (transverse anisotropic).

Each of the AC specimens involves 148 X-ray CT scan images, ignoring top and bottom slices. Three AC mixtures image slices consists of coarse, gap and fine aggregate sizes. The vector magnitude only address inclination angles of the aggregates while modified vector magnitude accounts aspect ratio, area and orientation of aggregates for each image slices with their average values for AC mixture is computed.

Figure 4.11, shows the average Vector and modified Vector magnitude values for Top, Middle and Bottom Layers respectively. The average modified Vector magnitude values are greater than Vector magnitude values for three AC mixtures within AC layers. It indicates there is inherent anisotropy of the AC mixtures for both vector and modified vector magnitude values having the same AC mixtures within AC layers. The effect of compaction varies from top to bottom layer and due to segregation of AC mixtures. Due to this, the distribution of aggregates vary within height of AC layers. From the results, there is a decrease in both vector and modified vector magnitude value from Top, Middle and Bottom layers respectively.

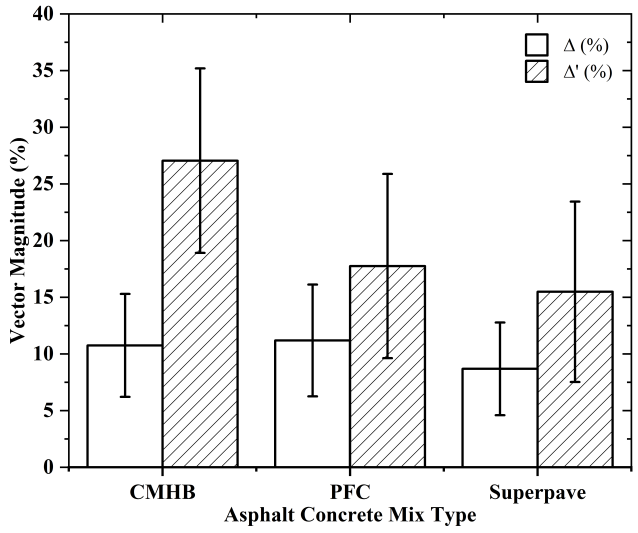

(a)

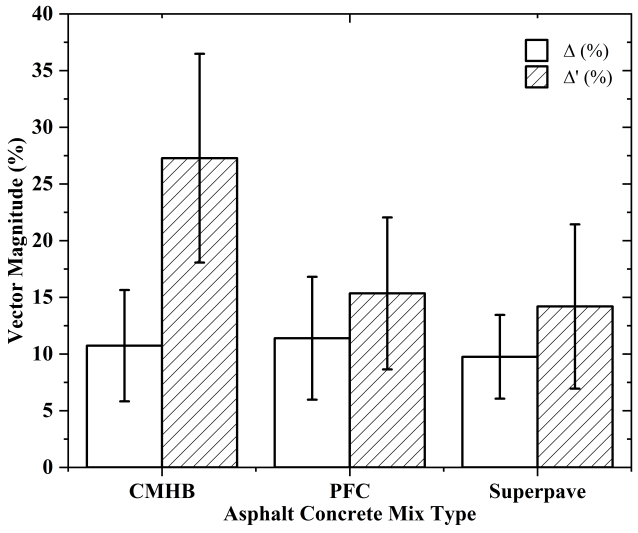

(b)

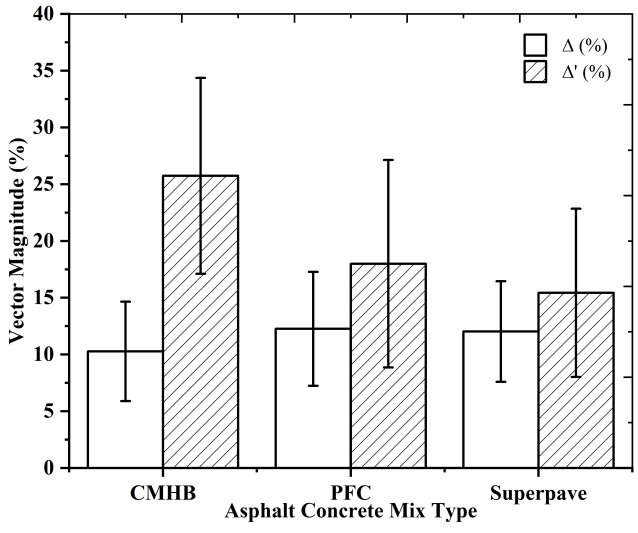

(c)

Figure 4.11: Vector and modified Vector Magnitude values: (a) Top (b) Middle and (c) Bottom.

Figure 4.12, shows Vector magnitude values for three AC mixtures within Top, Middle and Bottom AC layers. The Vector magnitude values for top, middle and bottom AC layers are relatively indicates the same value. However, Vector magnitude values for PFC mixture is relatively greater value than the other AC mixtures. Because, for PFC AC mixtures the composition of coarse aggregates greater than the the other AC mixtures. By considering only aggregate orientation the value of vector magnitude increases by decreasing sample specimen height of AC mixtures. Visually for three AC mixtures the values of Vector Magnitude within Top, Middle and Bottom Layers have same values. It indicates only aggregate Orientation do not properly indicate inherent anisotropy.

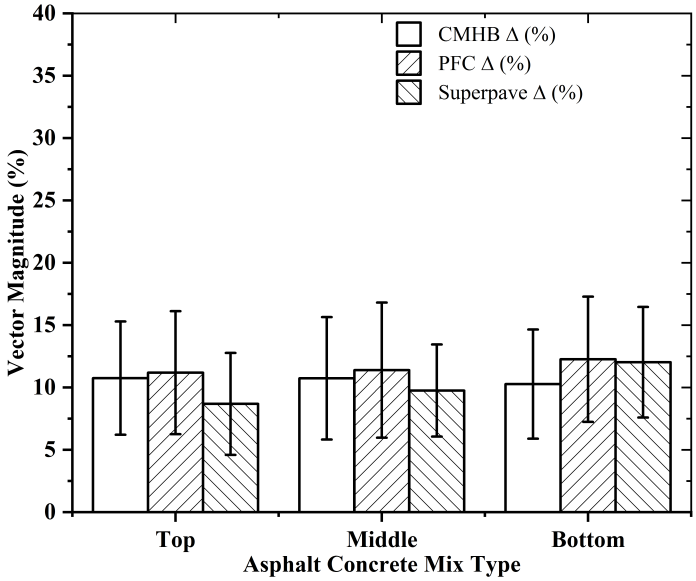

Figure 4.12: Vector magnitude values within AC layers for three AC mixtures.

Figure 4.13, shows modified Vector magnitude values for three AC mixtures within AC layers. There is variation in modified Vector magnitude within top, middle and bottom layers for three AC mixtures. Modified Vector magnitude values for CMHB AC mixture is relatively greater value than PFC and Superpave AC mixtures. By considering orientation, aspect ratio and area of aggregate the value of modified Vector magnitude is greater for Top and Bottom Layers of AC as compared to Middle layer of AC mixtures. It indicates anisotropy is greater in Top and Bottom layers relative to middle layers for three AC mixtures. Because, the effect of compaction was greatly affects on top of AC mixtures. In addition, due to segregation; coarse aggregates are found in Top and Bottom layers than Middle layers of AC mixtures.

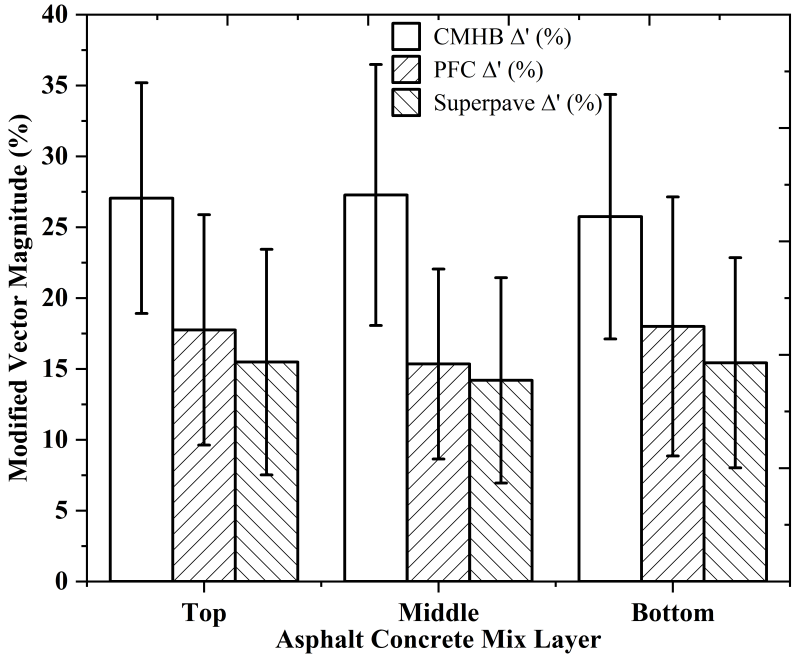

Figure 4.13: Modified Vector magnitude values within AC layers for three AC mixtures.

Figure 4.14, shows on the average Vector and modified Vector magnitude values for three AC mixtures. Modified Vector magnitude values shall be a good indicator to identify inherent anisotropy. From the three AC mixtures; CMHB have greater modified vector magnitude value than the others. It indicates anisotropy increases when aggregate is coarser. While, anisotropy decreases when the aggregate is finner. Due to this, Superpave Type C AC mixtures have smaller modified Vector magnitude values than the other AC mixtures. Because, the effect of aggregate morphological properties such as aspect ratio and area have negligible effect than coarse and gap graded AC mixtures. Visually for three AC mixtures the values of modified Vector Magnitude within Top, Middle and Bottom Layers have different values. It indicates aggregate Orientation, area and aspect ratio properly indicate inherent anisotropy. While, considering only aggregate orientation doesn't indicate inherent anisotropy.

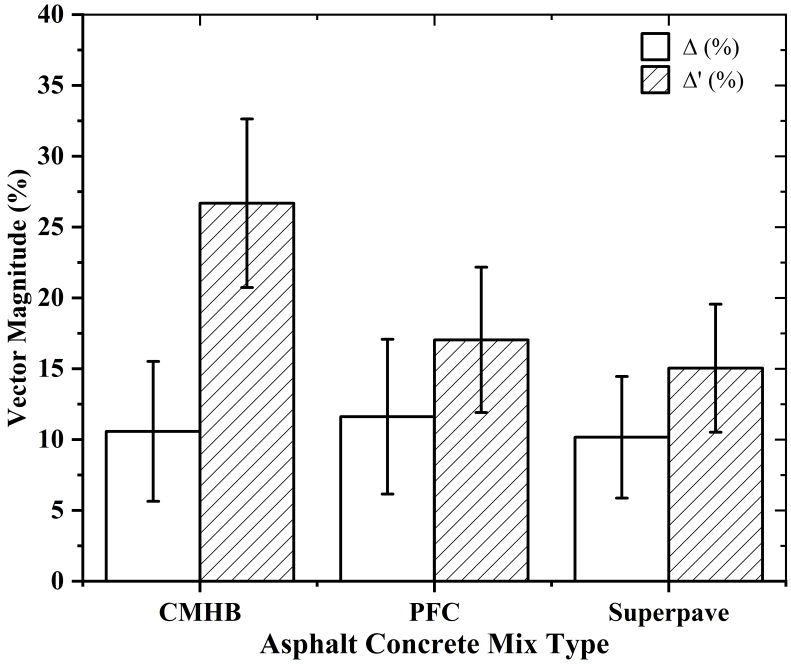

Figure 4.14: Average Vector and modified Vector Magnitude values.

The distribution of Vector and modified Vector magnitude along the specimen height for each Unaged three AC mixtures were presented below. Figure 4.15, shows distribution of Vector magnitude values over specimen height for CMHB, PFC and Superpave Type C AC mixtures, respectively. The maximum value of Vector magnitude over specimen height for CMHB and PFC have 0.25 while for Superpave have a value of 0.2. This finding is also agrees with past studies [37]. The CMHB and PFC AC mixtures exhibited uniformly distributed aggregates compared to Superpave mixture over specimen height. Hence, PFC is Gap-graded aggregate there is uniform textures in exposed aggregate concrete.

For CMHB Type C AC mixture, the distribution of Vector magnitude over Specimen Height are uniformly oriented. It indicates the gradation of aggregate includes both fine and coarse aggregates are uniformly distributed over Specimen Height. For PFC AC mixture, the distribution of Vector magnitude over Specimen Height are scatter. It indicates the gradation of aggregate are gap gadded which indicates the tendency to separate or scatter aggregates within Specimen Height. For Superpave Type C AC mixtures, the distribution of Vector magnitude over Specimen Height are cluster oriented having minimum Vector magnitude values. It indicates the tendency to inherently anisotropic was smaller for fine aggregate AC mixtures.

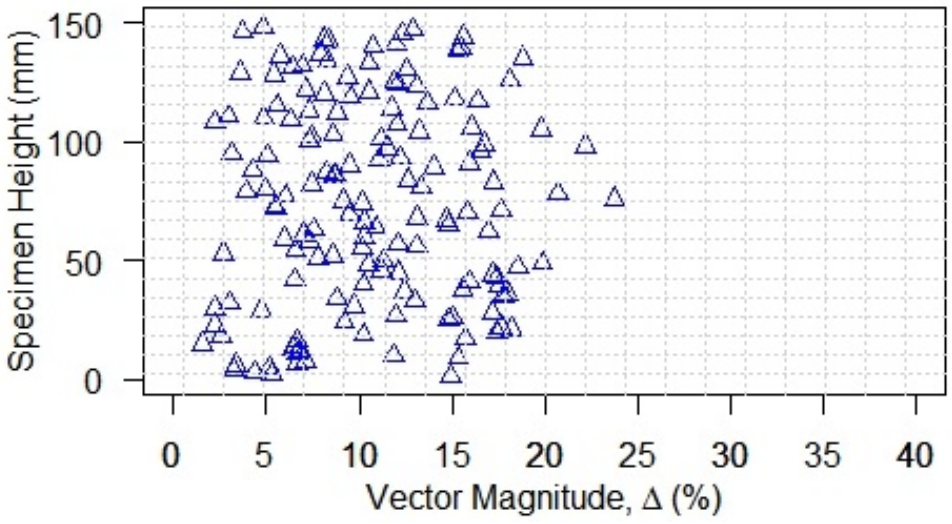

(a)

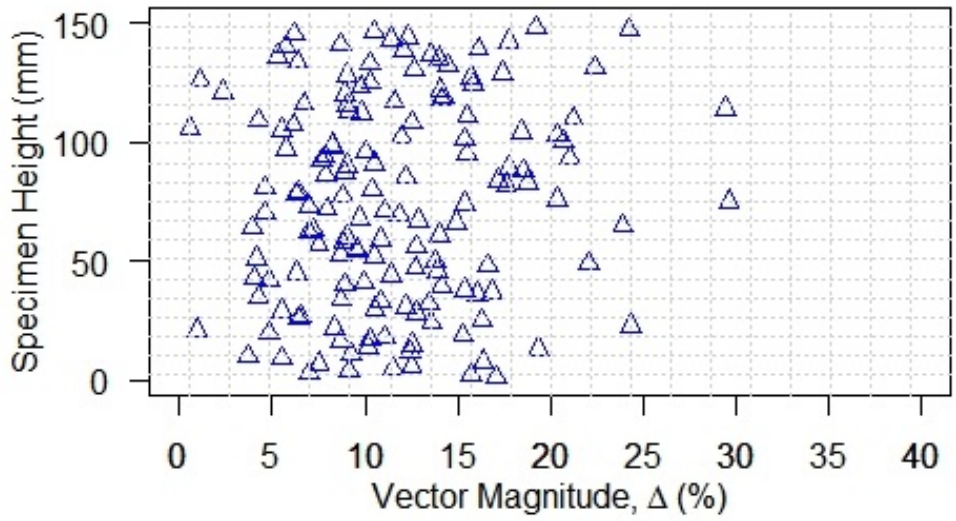

(b)

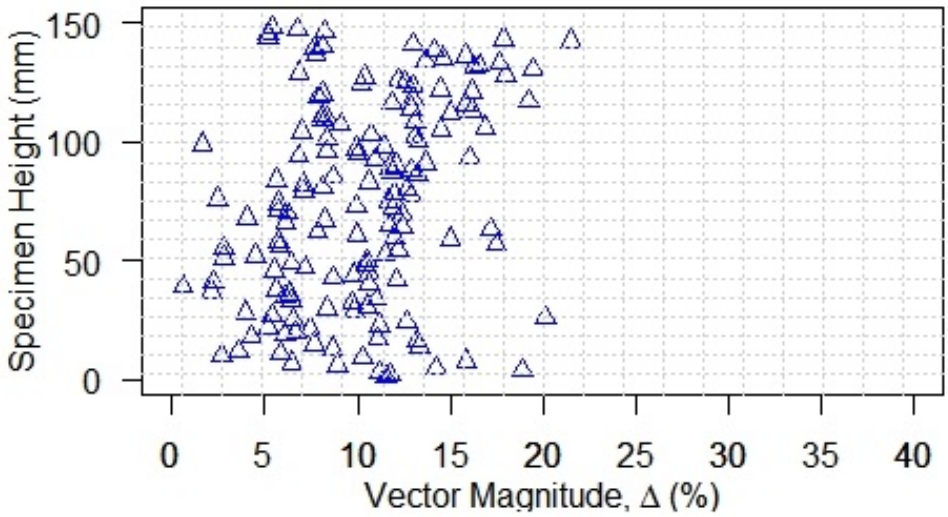

(c)

Figure 4.15: Distribution of Vector Magnitude over Specimen Height (a) CMHB (b) PFC and (c) Superpave.

Figure 4.16, show distribution of modified Vector magnitude values over specimen height for CMHB, PFC and Superpave Type C AC mixtures, respectively. The maximum value of modified Vector magnitude over specimen height for CMHB have 0.6, PFC have 0.5 and Superpave have a value of 0.35. By visual inspection, CMHB and Superpave exhibited uniformly distributed aggregates compared to PFC AC mixtures over specimen height. Vector magnitude were significantly smaller than modified vector magnitude demonstrates that the original formulation of vector magnitude substantially underestimates the inherent anisotropy of the AC mixtures. In other words, orientation of aggregates is not sufficient to quantify the inherent anisotropy of AC mixtures. The size and sphericity of the aggregates must be addressed to more accurately quantify the mixture's inherent anisotropy.

For CMHB Type C AC mixture, the distribution of modified Vector magnitude over Specimen Height are scatter everywhere. It indicates considering aggregate Orientation, area and aspect ratio indicates uniform inherent anisotropy over specimen Height for mixtures having fine and coarse aggregates. For PFC AC mixture, the distribution of modified Vector magnitude over Specimen Height are slightly scatter especially, for top and bottom part of AC mixtures. It indicates the tendency to segregate or scatter within top and bottom part of AC mixtures. For Superpave Type C AC mixtures, the distribution of modified Vector magnitude over Specimen Height are dense having minimum Vector magnitude values as compared to PFC AC mixtures. It indicates the tendency to inherently anisotropic was smaller for fine graded AC mixtures.

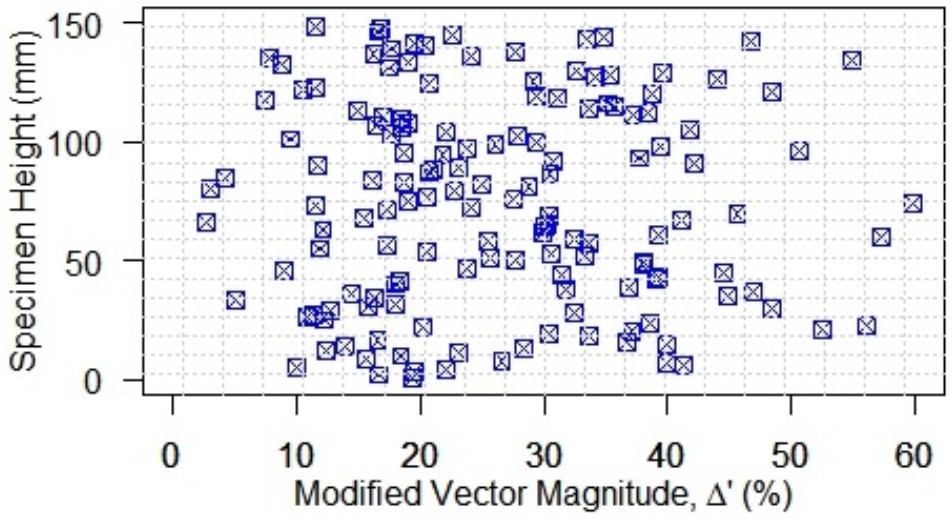

(a)

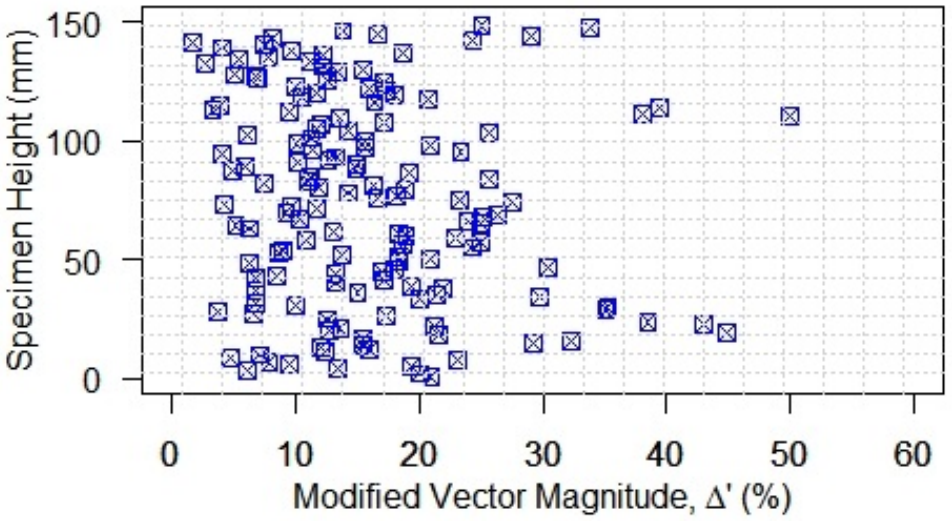

(b)

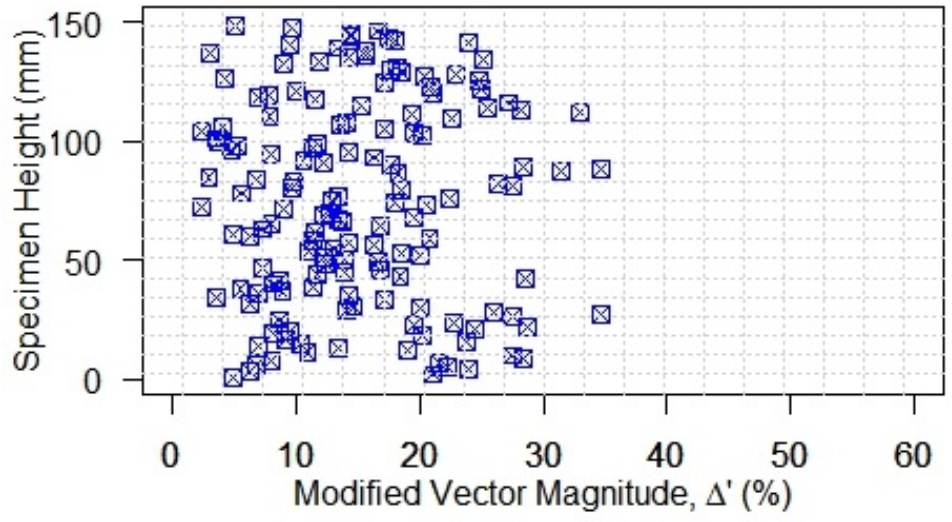

(c)

Figure 4.16: Distribution of modified Vector magnitude over Specimen Height (a) CMHB (b) PFC and (c) Superpave.

Comparing Δ and $\Delta^{'}$ in Figure 4.15 and 4.16, the value of $\Delta^{'}$ is significantly larger than the value of Δ; in certain cases, they are not even in the same order. This finding agrees with [37]. A smaller value of the vector magnitude indicates that the aggregates are more randomly distributed in the mixture so the mixture is less anisotropic while a larger value of the vector magnitude indicates that the aggregates are more horizontally oriented. Sample aggregate morphological characteristics of the horizontal slice three AC mixtures are given on Appendix C.

Relationship Between Vector Magnitude and Physical Properties

In order to analyze aggregate orientation and quantify inherent anisotropy in AC mixture, theoretical derivation between modified Vector magnitude Δ' and modulus ratio was developed by [37], which is given by Equation 2.10. Subsequently, he verify experimentally based on horizontal and vertical modulus results.

In order to relate vector magnitude to the physical properties like complex modulus we need vertical complex modulus (E^*_{11}) and horizontal complex modulus (E^*_{22}) data's which are done under frequency in between 0.05Hz-50Hz. Hence, our title is on inherent anisotropy, experimental tests shall be done less than or under 100 microstrains to relate vector magnitude with modulus ratio. Equation 2.10, is used together with the non destructive testing data on the field pavement sections to predict the horizontal modulus of the field pavement in the entire project length.

As can be seen from Figure 4.15 and 4.16, CMHB AC mixture have higher vector magnitude values than PFC and Superpave AC mixtures. Which leads, a higher value of vector magnitude is associated with a larger modulus ratio, which indicates a stronger anisotropy of the specimen. The modulus ratio is found solely on the modified vector magnitude that is a measure of the size, orientation of the aggregate particles. These aggregate characteristics are the inherent properties of the asphalt mixture; they determine the level of the inherent anisotropy of the mixture. In contrast, the modulus ratio is independent of the type of the asphalt binder, air void content and mixture aging period.

4.2 Statistical Analysis

The one-way analysis of variance allows us to compare several groups of observations, all of which are independent and possibly with a different mean for each group. The image analysis results were statistically analyzed for three AC mixtures. Here, we consider three AC mixtures (i.e., CMHB, PFC and Superpave).

ANOVA: Analysis of Variance Results

Below are ANOVA outputs for orientation, vector magnitude and modified vector magnitude values within top, middle and bottom layers of AC mixtures.

Null Hypothesis (H_o): $\mu_1 = \mu_2 = \mu_3$; there is no mean difference in the mean value within top, middle and bottom layers.

Alternate Hypothesis (H_a): $\mu_1 \neq \mu_2 \neq \mu_3$; at least one mean is different within top, middle and bottom layers.

$\alpha = 0.05$, so if p value < α: reject H_o or If F is in the rejection region, reject H_o. Otherwise, fail to reject H_o.

Confidence Interval (%): 95

Table 4.1, summary on Aggregate orientation, Vector and modified Vector magnitude was presented for three AC mixtures. For three AC mixtures; there is significant variation in orientation and Vector magnitude values is explained within Top, Middle and Bottom layers of AC mixtures at $\alpha = 5\%$ significance level. It leads having constant compaction pressure there is variation of aggregate properties. While, for modified vector magnitude values there is no significant variation within AC layers at $\alpha = 5\%$ significance level. When, there is significant variation within AC layers; multiple comparison test were performed using Scheffe's test which is presented on Appendix D, E and F for Aggregate orientation, Vector Magnitude and modified Vector magnitude respectively.

Table 4.1: Statistical analysis for Horizontal aggregate morphological properties.

Parameters	Mix. Type	F value	P value	Remark
Orientation (θ)	CMHB	0.46	0.634	Not significant
	PFC	3.86	0.023	Significant
	Superpave	9.93	0.00	Significant
Vector Magnitude (Δ)	CMHB	0.16	0.856	Not significant
	PFC	0.54	0.584	Not significant
	Superpave	8.63	0.000	Significant
Modified Vector Magnitude (Δ')	CMHB	0.19	0.824	Not significant
	PFC	0.40	0.669	Not significant
	Superpave	0.46	0.631	Not significant

Chapter 5

Conclusion and Recommendations

5.1 Conclusions

Image Processing is a field with a heavy impact on today's technology and tomorrow's way of life. It provides a major advantages as it is a cost effective, time efficient and non-destructive approach. There are three AC mixture designs: Coarse Matrix High Binder Type C (CMHB), Porous Friction Course (PFC) and a Superpave Type C AC mixtures [33]. Each of mixing designs has a PG 76-22 modified binder meeting, the Texas DOT specifications prepared with Hard Limestone aggregate. Three mixtures are compacted at 600 kPa ram pressure, placed at an angle of 1.25° and 30 gyration per minute using SGC. The X-ray CT was used to scan the AC performance specimens (100 mm diameter and 150 mm height).

The analysis was based on detecting and quantifying AC materials, i.e. aggregate orientation that can affect the behavior of AC by using image analysis of X-ray CT images. An Automated image processing algorithm was developed, using Adaptive Enhanced based Thresholding Algorithm (AETA) to process the scanned images and effectively separate connected or overlapping coarse and fine aggregate sizes ranging from 1.18mm to 19mm. Using the separated aggregates *MATLAB*® software, built in functions *bwboundaries* and *regionprops* quantify aggregate morphological properties such as area, equivalent diameter, perimeter, major axis length, minor axis length, and orientation [16].

The major axis inclination of horizontal axis was used to determine the orientation, which in turn was used to index the Vector magnitude of aggregate particles. In addition, it is used to determine orientation, Aspect ratio and Area of aggregates was used to know the index of the modified Vector magnitude of aggregate particles. Aggregate orientation was statistically analyzed for three AC mixtures. ANOVA was done to study the variability in image analysis results. On the basis of numerical analysis of this study, the following preliminary conclusions can be made based on the primary objectives and the methodology that we adopted:

- X-ray CT images are used to evaluate AC mixtures microstructural properties using image analysis. AC microstructural phases (Aggregate, air void and mastic phases) are used as an input for image-based analysis using (i.e., $MATLAB^{®}$) softwares on understanding the performance of AC mixtures. The analysis was used to measure the orientation, area and aspect ratio of the aggregates, which are then employed to calculate microstructural parameter.
- Average aggregate orientation value shows that approximately 20% of the aggregates have an inclination angle between -10^o-10^o, 65% of the aggregates have an inclination between -45^o-45^o, and 15% of aggregates have an inclination angle between -45^o-90^o for three AC mixtures. Small inclination angle indicates the aggregates lies flat in the horizontal direction. It demonstrates that the aggregates have a preferential distribution in the horizontal direction that is perpendicular to the compaction direction.
- The distribution of Vector magnitude over Specimen Height is uniformly oriented while, for modified Vector magnitude the distribution is scatter everywhere for CMHB Type C AC mixture. It indicates the gradation of aggregate includes both fine and coarse aggregates are uniformly distributed over Specimen Height.
- The distribution of Vector magnitude over Specimen Height is a scatter while, for modified Vector magnitude the distribution is slightly scatter, especially for top and bottom part of PFC AC mixture. It indicates that the tendency to separate or scatter aggregates within Specimen Height influenced due to gradation of aggregate (i.e., gap gadded).
- The distribution of Vector magnitude over Specimen Height is cluster oriented while, for modified Vector magnitude the distribution is dense having minimum Vector magnitude values for Superpave Type C AC mixtures. It indicates the composition of fine aggregates within superpave Type C AC mixture is greater. Due to this, their is smaller value of vector magnitude.

- The PFC and CMHB Type C exhibited randomly distributed aggregates compared to Superpave Type C AC mixture depending on the average value of Vector magnitude. A smaller value of the Vector magnitude indicates that the aggregates are more randomly distributed in the mixture so the mixture is less anisotropic while a larger value of the Vector magnitude indicates that the aggregates are more horizontally oriented.
- From the results, CMHB Type C AC mixture has higher Vector magnitude values than PFC and Superpave Type C AC mixtures. Because, CMHB Type C is composed of coarse graded aggregates compared to superpave Type C AC mixtures and segregation is more prominent on gap graded PFC AC mixture. It indicates a higher value of modulus ratio, leads a stronger anisotropy of the specimen.
- The modulus ratio solely depends on the aggregate characteristics, including the inclination angle, size and sphericity while it is independent of the asphalt binder type, air void content and aging period. This relationship successfully serves as a bridge between the physical properties and anisotropy of the AC mixtures.
- Statistical analysis was performed to measure the inherent anisotropy of AC mixtures due to constant compaction pressure. From this aggregate orientation varies within Top, Middle and Bottom Layers of AC mixtures. Scheffe multi comparison tests were performed to know the variation of the orientation for AC mixtures. So, we can conclude that aggregates having constant compaction pressure, number of gyration and gyration angle inhibit differences in orientation which evaluates inherent anisotropy in AC mixtures.

Generally, image analysis assists in identifying the difference between the design & actual condition, automatically detects and recognizing the damage (in pavements, structural members) and resolve disputes (when utilized as evidence). Due to this, we can predict the performance of AC mixtures i.e Mechanistic Empirical Approach which is current experimental techniques. Finally, it is concluded that this project helped to strengthen programming skills, expand knowledge of *MATLAB*® and image processing theory. This scope provides a basis for developing a larger project whose scope will be a tool for the study of 3D tomography asphalt specimens. Such study is a subject of ongoing investigation.

5.2 Recommendations

In order to study such type of research; we recommend the following concerned companies by considering the effort of each student;

- We would recommend partly to Addis Ababa Science and Technology University (AASTU) to get access to laboratory tests. In addition, the application of Numerical approaches in Highway Engineering may include to the curriculum and give such numerical software to simulate such tests numerically.
- We would recommend the Ethiopian Road Authority (ERA), Addis Ababa City Road Authority (AACRA) and Ministry of Transport (MoT): as we see from conclusion aggregate morphological properties are more descriptive than Volumetric properties (i.e., density of material). It indicates we want to change our pavement design philosophy (from Empirical to Mechanistic-Empirical Pavement Design Guide) to produce economical and safe (both structural and functionally (i.e., dependent on aggregates)) roads. This is used to detect and recognize damage in (both pavements, structural members) and resolve disputes when used as evidence.

5.3 Future Study

Considering the above mentioned research, the future scope of the study may include the following:

- Using different compaction methods, varying compaction levels and angles of gyration.
- Use Numerical simulations methods to study stress-induced anisotropy.
- Changing the type of instrument to scan images, image resolution was 195 μm, any aggregates smaller than about sieve No. 70 could not be identified.
- Using Aged AC mixtures (i.e., 6 months and 1 years).
- Varying specimen height.

References

1. Chandan, C., Sivakumar, K., Masad, E. & Fletcher, T. Application of imaging techniques to geometry analysis of Aggregate particles. *Journal of computing in civil engineering* **18,** 75–82 (2004).
2. Coenen, A. R., Kutay, M. E., Sefidmazgi, N. R. & Bahia, H. U. Aggregate structure characterisation of Asphalt mixtures using two-dimensional image analysis. *Road Materials and Pavement Design* **13,** 433–454 (2012).
3. Cowin, S. C. The relationship between the Elasticity Tensor and the Fabric Tensor. *Mechanics of Materials* **4,** 137–147 (1985).
4. Curray, J. R. The analysis of two-dimensional orientation data. *The Journal of Geology* **64,** 117–131 (1956).
5. Dessouky, S. H. & Masad, E. A. *The development of a Microstructural-based continuum model for Hot Mix Asphalt* in *Asphalt Concrete Simulation, Modeling, and Experimental Characterization. American Society of Civil Engineers* (2006).
6. Gonzalez, R. & Woods, R. *Digital Image Processing* 2nd ed. ISBN: 9780131687288 (Pearson Prentice Hall, 2008).
7. Hu, C. *et al.* Characterization of Asphalt mixture homogeneity based on X-ray Computed Tomography. *Journal of Testing and Evaluation* **40,** 1082–1088 (2012).
8. Huang, B., Chen, X., Shu, X., Masad, E. & Mahmoud, E. Effects of coarse Aggregate angularity and Asphalt binder on laboratory-measured permanent deformation properties of HMA. *International Journal of Pavement Engineering* **10,** 19–28 (2009).
9. John, C. A Computational approach to Edge Detection. *IEEE Transactions on Pattern Analysis and Machine Intelligence* **8** (1986).
10. Kim, S.-H. & Kim, N. Micromechanics analysis of Granular soils to estimate inherent anisotropy. *KSCE Journal of Civil Engineering* **11,** 145–149 (2007).

11. Kuo, C.-Y. & Freeman, R. B. Image analysis evaluation of aggregates for Asphalt Concrete mixtures. *Transportation Research Record* **1615,** 65–71 (1998).

12. Masad, E., Muhunthan, B., Shashidhar, N. & Harman, T. Internal structure characterization of Asphalt Concrete using image analysis. *Journal of computing in civil engineering* **13** (1999).

13. Masad, E. & Button, J. Implications of Experimental measurements and analyses of the internal structure of Hot Mix Asphalt. *Journal of the Transportation Research Board,* 212–220 (2004).

14. Masad, E., Olcott, D., White, T. & Tashman, L. Correlation of fine aggregate imaging shape indices with Asphalt mixture performance. *Transportation Research Record* **1757,** 148–156 (2001).

15. Masad, E., Tashman, L., Somedavan, N. & Little, D. Micromechanics-based analysis of stiffness anisotropy in Asphalt mixtures. *Journal of Materials in Civil Engineering* **14,** 374–383 (2002).

16. Mathworks, P. *MATLAB Guide: Image Processing Toolbox* https://www.mathworks.com/products/image.html (2019).

17. Monismith, C. L. *Analytically based Asphalt Pavement Design and rehabilitation: Theory to practice, 1962-1992* **1354** (1992).

18. Oda, M. Inherent and induced anisotropy in plasticity theory of Granular soils. *Mechanics of Materials* **16,** 35–45 (1993).

19. Oda, M. Initial fabrics and their relations to mechanical properties of Granular material. *Soils and foundations* **12,** 17–36 (1972).

20. Oda, M. & Nakayama, H. Yield function for soil with anisotropic fabric. *Journal of Engineering Mechanics* **115,** 89–104 (1989).

21. Pan, T., Tutumluer, E. & Carpenter, S. H. Effect of coarse Aggregate Morphology on permanent deformation behavior of Hot Mix Asphalt. *Journal of transportation engineering* **132,** 580–589 (2006).

22. Papagiannakis, T., Zelelew, H. & Agaian, S. in *Asphalt Pavements* 565–574 (CRC Press, 2014).

23. Saadeh, S., Masad, E. & Little, D. Characterization of Asphalt mix response under repeated loading using anisotropic nonlinear Viscoelastic-Viscoplastic model. *Journal of Materials in Civil Engineering* **19,** 912–924 (2007).

24. Sousa, J. B., Craus, J. & Monismith, C. L. *Summary report on Permanent deformation in Asphalt Concrete* tech. rep. (1991).

25. Tashman, L., Masad, E., Little, D. & Zbib, H. A microstructure-based viscoplastic model for Asphalt Concrete. *International Journal of Plasticity* **21,** 1659–1685 (2005).

26. Tobita, Y. & Yanagiswa, E. Modified Stress Tensors for anisotropic behavior of Granular materials. *Soils and Foundations* **32,** 85–99 (1992).

27. Underwood, S., Heidari, A. H., Guddati, M. & Kim, Y. R. Experimental investigation of anisotropy in Asphalt Concrete. *Transportation research record* **1929,** 238–247 (2005).

28. Wan, R. G. & Guo, P. J. Stress Dilatancy and Fabric dependencies on sand behavior. *Journal of Engineering Mechanics* **130,** 635–645 (2004).

29. Wang, L.-B. Mechanics of Asphalt: Microstructure and Micromechanics. *International Journal of Pavement Research and Technology* **5** (2012).

30. Wang, L., Hoyos, L. R., Wang, J., Voyiadjis, G. & Abadie, C. Anisotropic Properties of Asphalt Concrete: characterization and implications for pavement design and analysis. *Journal of materials in civil engineering* **17,** 535–543 (2005).

31. Yoder, E. J., Witczak, M. W., *et al. Principles of Pavement Design* (John Wiley & Sons, 1975).

32. Yue, Z. Q., Bekking, W. & Morin, I. Application of Digital Image Processing to quantitative study of Asphalt Concrete microstructure. *Transportation Research Record* **1492,** 53–60 (1995).

33. Zelelew, H. M. *Simulation of the permanent deformation of Asphalt Concrete mixtures using Discrete Element Method (DEM) (PhD Dissertation)* **08** (Washington State University, Pullman, WA, 2008).

34. Zelelew, H. & Papagiannakis, T. *Characterization of Asphalt Concrete Microstructure using a Volumetrics-Based Thresholding Algorithm* 2010.

35. Zelelew, H., Almuntashri, A., Agaian, S. & Papagiannakis, A. An improved image processing technique for Asphalt Concrete X-ray CT images. *Road Materials and Pavement Design* **14,** 341–359 (2013).

36. Zelelew, H., Papagiannakis, A. & Masad, E. *Application of Digital Image Processing techniques for Asphalt Concrete mixture images* in (2008), 119–124.

37. Zhang, Y., Luo, R. & Lytton, R. L. Microstructure-based inherent anisotropy of Asphalt mixtures. *Journal of Materials in Civil Engineering* **23,** 1473–1482 (2011).

Appendices

Appendix A: MATLAB Codes for Processing of Images

```
%++++++++++++++++++++++++++++++++++++++++++++++++++++++++++
%++  Analysis of Inherent Anisotropy in Asphalt Concrete Mixtures  ++
%++  Zekariyas Mussie Amanu[1] & Habtamu Melese Zelelew[2]  ++
% [1] MSc. Candidate College of Civil and Architecture Engineering, Addis Ababa Science and Technology University, Addis Ababa, e-mail: zekariyasmussie@gmail.com
% [2] Professor, Founder of Lucy Consulting Engineers PLC, Addis Ababa, e-mail: habtamu.zelelew@lucyconsulting.com
%++++++++++++++++++  Goal  ++++++++++++++++++
% This program was written to analyze the inherent anisotropy of AC mixtures for research purpose only using image processing toolbox MATLAB® built-in function called regionprops and bwbounderies.
%++++++++++++  Approach  ++++++++++++++++++
% First, Using MATLAB- Image Processing toolbox process images in order to ready images for analysis of Asphalt Concrete. Second, Using regionprops and bwboundaries detect Asphalt Concrete material especially, aggregate orientation.
% Given Two dimensional Asphalt Concrete X-Ray Commuted Tomography images are:
% HL CMHB: Hard Limestone Coarse Graded Coarse Matrix High Binder Type C, HL PFC: Hard Limestone Gap Graded Porous Friction Course and HL Superpave: Hard Limestone Fine Graded Superpave Type C
clc;
clear all;
close all;
format long g;
```

```
format compact;
fontSize = 25;
% PART 1 - Processing:
% Read Input Images
coarse = imread('HL CMHB.png');
porous = imread('HL PFC.png');
superpave = imread('HL Superpave.png');
coarse_resize = imresize(coarse, [518,350]);
coarse_resize = imresize(coarse, [518,350]);
coarse_resize = imresize(coarse, [518,350]);

% Display Input Image
figure;imshow(coarse_resize);title('InputCMHBTypeCImage');
figure;imshow(porous_resize);title('InputPFCImage');
figure;imshow(superpave_resize);title('InputSuperpaveTypeCImage');
% Contrast Enhancement using Histogram Equalization
figure;imshow(coarse_resize);title('InputCMHBTypeCImage');
figure;imhist(coarse_resize);title('HistogramforInputCMHBTypeCImage');
figure;imshow(porous_resize);title('InputPFCImage');
figure;imhist(porous_resize);title('HistogramforInputPFCImage');
figure;imshow(superpave_resize);title('InputSuperpaveTypeCImage');
figure;imhist(superpave_resize);title('HistogramforInputSuperpaveTypeCImage');
% Histogram Equalization
coarse_histeq = histeq(coarse_resize,256);
porous_histeq = histeq(porous_resize,256);
superpave_histeq = histeq(superpave_resize,256);
figure;imshow(coarse_histeq);title('HistogramequalizedCMHBTypeCImage');
figure;imhist(coarse_histeq);title('HistogramforEqualizedCMHBTypeCImage');
figure;imshow(porous_histeq);title('HistogramequalizedPFCImage');
figure;imhist(porous_histeq);title('HistogramforEqualizedPFCImage');
figure;imshow(superpave_histeq);title('HistogramequalizedSuperpaveTypeCImage');
figure;imhist(superpave_histeq);title('HistogramforEqualizedSuperpaveTypeCImag
% Noise removal by Median filtering
r = coarse_resize(:,:,1); g = coarse_resize(:,:,2); b = coarse_resize(:,:,3);
```

$r = imnoise(r,'salt\&pepper',0.02);\ g = imnoise(g,'salt\&pepper',0.02);$
$b = imnoise(b,'salt\&pepper',0.02);$
$NoisyImage(:,:,1) = r;\ NoisyImage(:,:,2) = g;NoisyImage(:,:,3) = b;$
$NoisyImage = uint8(NoisyImage);$
$figure;imshow(NoisyImage);title('NoisyCMHBTypeCImage');$

$r1 = NoisyImage(:,:,1);\ g1 = NoisyImage(:,:,2);\ b1 = NoisyImage(:,:,3);$
$r1 = medfilt2(r1,[3,3]);\ g1 = medfilt2(g1,[3,3]);\ b1 = medfilt2(b1,[3,3]);$
$FilteredImage(:,:,1) = r1;\ FilteredImage(:,:,2) = g1;$
$FilteredImage(:,:,3) = b1;\ FilteredImage = uint8(FilteredImage);$
$figure;imshow(FilteredImage);title('FilteredCMHBTypeCImage');$

$r = porous(:,:,1);\ g = porous(:,:,2);\ b = porous(:,:,3);$
$r = imnoise(r,'salt\&pepper',0.02);\ g = imnoise(g,'salt\&pepper',0.02);$
$b = imnoise(b,'salt\&pepper',0.02);$
$NoisyImage(:,:,1) = r;\ NoisyImage(:,:,2) = g;\ NoisyImage(:,:,3) = b;$
$NoisyImage = uint8(NoisyImage);$
$figure;imshow(NoisyImage);title('NoisyPFCImage');$

$r1 = NoisyImage(:,:,1);\ g1 = NoisyImage(:,:,2);\ b1 = NoisyImage(:,:,3);$
$r1 = medfilt2(r1,[3,3]);\ g1 = medfilt2(g1,[3,3]);\ b1 = medfilt2(b1,[3,3]);$
$FilteredImage(:,:,1) = r1;\ FilteredImage(:,:,2) = g1;$
$FilteredImage(:,:,3) = b1;\ FilteredImage = uint8(FilteredImage);$
$figure;imshow(FilteredImage);title('FilteredPFCImage');$

$r = superpave(:,:,1);\ g = superpave(:,:,2);\ b = superpave(:,:,3);$
$r = imnoise(r,'salt\&pepper',0.02);\ g = imnoise(g,'salt\&pepper',0.02);$
$b = imnoise(b,'salt\&pepper',0.02);$
$NoisyImage(:,:,1) = r;\ NoisyImage(:,:,2) = g;\ NoisyImage(:,:,3) = b;$
$NoisyImage = uint8(NoisyImage);$
$figure;imshow(NoisyImage);title('NoisySuperpaveImage');$

$r1 = NoisyImage(:,:,1);\ g1 = NoisyImage(:,:,2);\ b1 = NoisyImage(:,:,3);$
$r1 = medfilt2(r1,[3,3]);\ g1 = medfilt2(g1,[3,3]);\ b1 = medfilt2(b1,[3,3]);$
$FilteredImage(:,:,1) = r1;\ FilteredImage(:,:,2) = g1;$
$FilteredImage(:,:,3) = b1;\ FilteredImage = uint8(FilteredImage);$
$figure;imshow(FilteredImage);title('FilteredSuperpaveImage');$

% Edge Detection
$coarse\_canny = edge(coarse\_gray,'canny');$

```
figure;imshow(coarse_canny);title('CannyCMHBTypeCImage');
porous_canny = edge(porous_gray,'canny');
figure;imshow(porous_canny);title('CannyPFCImage');
superpave_canny = edge(superpave_gray,'canny');
figure;imshow(superpave_canny);title('CannySuperpaveTypeCImage');

% Image Segementation
coarse_se = strel('square',5)
porous_se = strel('square',5)
superpave_se = strel('square',5)
coarse_cannydil = imdilate(coarse_canny,coarse_se);
porous_cannydil = imdilate(porous_canny,porous_se);
superpave_cannydil = imdilate(superpave_canny,superpave_se);
figure;imshow(coarse_cannydil);title('DilatedCMHBTypeCImage');
figure;imshow(porous_cannydil);title('DilatedPFCImage');
figure;imshow(superpave_cannydil);title('DilatedSuperpaveTypeCImage');

coarse_cannyfill = imfill(coarse_cannydil,'holes');
porous_cannyfill = imfill(porous_cannydil,'holes');
superpave_cannyfill = imfill(superpave_cannydil,'holes');
figure;imshow(coarse_cannyfill);title('FillholesCMHBTypeCImage');
figure;imshow(porous_cannyfill);title('FillholesPFCImage');
figure;imshow(superpave_cannyfill);title('FillholesSuperpaveTypeCImage');

coarse_cannyopen = bwareaopen(coarse_cannyfill,50);
porous_cannyopen = bwareaopen(porous_cannyfill,50);
superpave_cannyopen = bwareaopen(superpave_cannyfill,50);
figure;imshow(coarse_cannyopen);title('RemovedSmallobjectCMHBTypeCImage');
figure;imshow(porous_cannyopen);title('RemovedSmallobjectPFCImage');
figure;imshow(superpave_cannyopen);title('RemovedSmallobjectSuperpaveTypeCIm

coarse_cc = bwconncomp(coarse_cannyfill);
porous_cc = bwconncomp(porous_cannyfill);
superpave_cc = bwconncomp(superpave_cannyfill);
coarse_L = labelmatrix(coarse_cc);
porous_L = labelmatrix(porous_cc);
superpave_L = labelmatrix(superpave_cc);
figure;imshow(ind2rgb(coarse_L, jet(5)));title('LabeledCMHBTypeCImage');
figure;imshow(ind2rgb(porous_L, jet(5)));title('LabeledPFCImage');
```

```
figure; imshow(ind2rgb(superpave_L, jet(5))); title('LabeledSuperpaveTypeCImage');

coarse_stats = regionprops(coarse_L,'Area');
porous_stats = regionprops(porous_L,'Area');
superpave_stats = regionprops(superpave_L,'Area');
coarse_idx = find([coarse_stats.Area] > 50);
porous_idx = find([porous_stats.Area] > 50);
superpave_idx = find([superpave_stats.Area] > 50);

coarse_cannyopen = ismember(coarse_L, coarse_idx);
porous_cannyopen = ismember(porous_L, porous_idx);
superpave_cannyopen = ismember(superpave_L, superpave_idx);
figure; imshow(coarse_cannyopen); title('FilteroutAreaCMHBTypeCImage');
figure; imshow(porous_cannyopen); title('FilteroutAreaPFCImage');
figure; imshow(superpave_cannyopen); title('FilteroutAreaSuperpaveTypeCImage');

coarse_cannyfinal = imerode(coarse_cannyopen, coarse_se);
porous_cannyfinal = imerode(porous_cannyopen, porous_se);
superpave_cannyfinal = imerode(superpave_cannyopen, superpave_se);
figure; imshow(coarse_cannyfinal); title('FinalErodedCMHBTypeCImage');
figure; imshow(porous_cannyfinal); title('FinalErodedPFCImage');
figure; imshow(superpave_cannyfinal); title('FinalErodedSuperpaveTypeCImage');

coarse_cannyoutline = bwperim(coarse_cannyfinal);
porous_cannyoutline = bwperim(porous_cannyfinal);
superpave_cannyoutline = bwperim(superpave_cannyfinal);
figure; imshow(coarse_cannyoutline); title('PerimeterCMHBTypeCImage');
figure; imshow(porous_cannyoutline); title('PerimeterPFCImage');
figure; imshow(superpave_cannyoutline); title('PerimeterSuperpaveTypeCImage');

coarse_y = coarse_canny;
porous_y = porous_canny;
superpave_y = superpave_canny;
coarse_y(coarse_cannyoutline) = 255;
porous_y(coarse_cannyoutline) = 255;
superpave_y(coarse_cannyoutline) = 255;
figure; imshow(coarse_y); title('FinalSegementedCMHBTypeCImage');
figure; imshow(porous_y); title('FinalSegementedPFCImage');
figure; imshow(superpave_y); title('FinalSegementedSuperpaveTypeCImage');
```

Appendix B: MATLAB Codes for Analysis of Images

```
% HL CMHB Type C (Hard Limestone Coarse Matrix High Binder Type C)
function_im = Thresholding(coarse_gray)
[r,c] = size(coarse_gray);
im = zeros(r,c);
for i = 1 : r
for j = 1 : c
if coarse_gray(i, j) > 105
im(i, j) = 1;
end
end
end
im = bwareaopen(im,5);
im = imfill(im,'holes');
end

coarse_threshold = Thresholding(coarse_gray);
cc = bwconncomp(coarse_threshold,8)
n = cc.NumObjects;
Area = zeros(n,1);
Perimeter = zeros(n,1);
MajorAxis = zeros(n,1);
MinorAxis = zeros(n,1);
k = regionprops(coarse_gray,'Area','Perimeter','MajorAxisLength','MinorAxisLength'

for i = 1 : n
Area(i) = k(i).Area;
Perimeter(i) = k(i).Perimeter;
MajorAxis(i) = k(i).MajorAxisLength;
MinorAxis(i) = k(i).MajorAxisLength;
Orientation(i) = k(i).Orientation;
EquivDiameter(i) = k(i).EquivDiameter;
end

graindata(1,1) = mean(Area);
graindata(2,1) = mean(Perimeter);
graindata(3,1) = mean(MajorAxis);
```

```
graindata(4,1) = mean(MinorAxis);
graindata(5,1) = mean(Orientation);
graindata(6,1) = mean(EquivDiameter);
col_header = 'Area','Perimeter','MajorAxisLength','MinorAxisLength','Orientation','
xlswrite('cmhb.xlsx',[Area(:),Perimeter(:),MajorAxis(:),MinorAxis(:
),Orientation(:),EquivDiameter(:)],'sheet1','A2');
xlswrite('cmhb.xlsx',col_header,'sheet1','A1');

% HL PFC (Hard Limestone Gap Graded Porous Friction Coarse)
function_im = Thresholding(porous_gray) [r,c] = size(porous_gray);
im = zeros(r,c);
for i = 1 : r
for j = 1 : c
if porous_gray(i, j) > 55
im(i, j) = 1;
end
end
end
im = bwareaopen(im,5);
im = imfill(im,'holes');
end

porous_threshold = Thresholding(porous_gray);
cc = bwconncomp(porous_threshold,8)
n = cc.NumObjects;
Area = zeros(n,1);
Perimeter = zeros(n,1);
MajorAxis = zeros(n,1);
MinorAxis = zeros(n,1);
k = regionprops(porous_gray,'Area','Perimeter','MajorAxisLength','MinorAxisLength'
for i = 1 : n
Area(i) = k(i).Area;
Perimeter(i) = k(i).Perimeter;
MajorAxis(i) = k(i).MajorAxisLength;
MinorAxis(i) = k(i).MajorAxisLength;
Orientation(i) = k(i).Orientation;
EquivDiameter(i) = k(i).EquivDiameter;
```

```
end
graindata(1,1) = mean(Area);
graindata(2,1) = mean(Perimeter);
graindata(3,1) = mean(MajorAxis);
graindata(4,1) = mean(MinorAxis);
graindata(5,1) = mean(Orientation);
graindata(6,1) = mean(EquivDiameter);
col_header = 'Area','Perimeter','MajorAxisLength','MinorAxisLength','Orientation','
xlswrite('PFC.xlsx',[Area(:),Perimeter(:),MajorAxis(:),MinorAxis(:
),Orientation(:),EquivDiameter(:)],'sheet1','A2');
xlswrite('PFC.xlsx',col_header,'sheet1','A1');
% HL Superpave Type C ( Hard Limestone Superpave Type C)
function_im = Thresholding(superpave_gray)
[r,c] = size(superpave_gray);
im = zeros(r,c);
for i = 1 : r
for j = 1 : c
if superpave_gray(i, j) > 55
im(i, j) = 1;
end
end
end
im = bwareaopen(im,5);
im = imfill(im,'holes');
end
superpave_threshold = Thresholding(superpave_gray);
cc = bwconncomp(superpave_threshold,8)
n = cc.NumObjects;
Area = zeros(n,1);
Perimeter = zeros(n,1);
MajorAxis = zeros(n,1);
MinorAxis = zeros(n,1);
k = regionprops(superpave_gray,'Area','Perimeter','MajorAxisLength','MinorAxisLen
for i = 1 : n
Area(i) = k(i).Area;
```

$Perimeter(i) = k(i).Perimeter;$
$MajorAxis(i) = k(i).MajorAxisLength;$
$MinorAxis(i) = k(i).MajorAxisLength;$
$Orientation(i) = k(i).Orientation;$
$EquivDiameter(i) = k(i).EquivDiameter;$
end

$graindata(1,1) = mean(Area);$
$graindata(2,1) = mean(Perimeter);$
$graindata(3,1) = mean(MajorAxis);$
$graindata(4,1) = mean(MinorAxis);$
$graindata(5,1) = mean(Orientation);$
$graindata(6,1) = mean(EquivDiameter);$
$col\_header = 'Area','Perimeter','MajorAxisLength','MinorAxisLength','Orientation','I$
$xlswrite('Superpave.xlsx',[Area(:),Perimeter(:),MajorAxis(:$
$),MinorAxis(:),Orientation(:),EquivDiameter(:)],'sheet1','A2');$
$xlswrite('Superpave.xlsx',col\_header,'sheet1','A1');$

Appendix C: Aggregate Morphological Properties

Table 5.1: CMHB Horizontal slice No. 8 AC mixture Aggregate Properties.

Area (mm^2)	Major Axis (mm)	Minor Axis (mm)	θ (^{o})	Equ. Diameter (mm)
378	42.010	14.528	85.769	21.938
37	8.162	6.026	-65.545	6.863
2409	68.635	46.948	56.303	55.382
258	33.008	13.571	-12.892	18.124
363	24.230	20.756	-88.505	21.499

Table 5.2: PFC Horizontal slice No. 8 AC mixture Aggregate Properties.

Area (mm^2)	Major Axis (mm)	Minor Axis (mm)	θ (^{o})	Equ. Diameter (mm)
1131	51.059	29.210	-73.871	37.948
157	14.245	14.245	0	14.139
293	22.085	17.120	-70.716	19.315
6196	120.406	87.270	78.641	88.819
2162	71.070	39.126	-27.546	52.467

Table 5.3: Superpave Horizontal slice No. 8 AC mixture Aggregate Properties.

Area (mm^2)	Major Axis (mm)	Minor Axis (mm)	θ (^{o})	Equ. Diameter (mm)
306	33.358	18.239	2.099	19.739
65	12.505	7.085	46.867	9.097
71	11.938	8.001	89.282	9.508
51	10.935	6.236	50.761	8.058
24	6	5.454	0	5.528

Table 5.4: Sample Horizontal slice θ, M, Δ & Δ' values for CMHB AC mixture.

Slice No.	M	$\theta(^o)$	$\Delta(\%)$	$\Delta'(\%)$
1	191	39.370	14.928	19.406
2	206	42.420	5.287	16.673
3	178	43.123	4.392	19.428
4	167	45.173	3.286	22.001

Table 5.5: Sample Horizontal slice for θ, M, Δ & Δ' values for PFC AC mixture.

Slice No.	M	$\theta(^o)$	$\Delta(\%)$	$\Delta'(\%)$
1	74	38.522	17.119	20.957
2	70	39.276	15.755	19.971
3	67	42.724	7.014	6.073
4	68	45.086	9.169	13.309

Table 5.6: Sample Horizontal slice θ, M, Δ & Δ' values for Superpave AC mixture.

Slice No.	M	$\theta(^o)$	$\Delta(\%)$	$\Delta'(\%)$
1	296	40.263	11.562	4.925
2	243	40.155	11.776	21.107
3	244	40.765	11.165	6.310
4	194	39.576	18.910	23.910

Appendix D: Aggregate Orientation

Table 5.7: CMHB: ANOVA results for Aggregate Orientation.

Source of Variation	Sum of Squares	df	Mean Squares	F value	Prob. > F value	$F_{critical}$
Between Groups	5.109	2	2.554	0.46	0.634	3.068
Within Groups	809.935	145	5.586	-	-	-
Total	815.043	147	-	-	-	-

Table 5.8: PFC: ANOVA results for Aggregate Orientation.

Source of Variation	Sum of Squares	df	Mean Squares	F value	Prob. > F value	$F_{critical}$
Between Groups	100.058	2	50.029	3.86	0.023	3.068
Within Groups	1877.174	145	12.946	-	-	-
Total	1977.232	147	-	-	-	-

Table 5.9: PFC: Scheffe results for Aggregate Orientation.

Row Mean - Col. Mean	Top Layer	Middle Layer
Middle Layer	-1.540 0.110	-
Bottom Layer	0.356 0.886	1.896 0.035

Table 5.10: Superpave: ANOVA results for Aggregate Orientation.

Source of Variation	Sum of Squares	df	Mean Squares	F value	Prob. > F value	$F_{critical}$
Between Groups	52.469	2	26.235	9.93	0.000	3.068
Within Groups	382.962	145	2.641	-	-	-
Total	435.432	147	-	-	-	-

Table 5.11: Superpave: Scheffe results for Aggregate Orientation.

Row Mean - Col. Mean	Top Layer	Middle Layer
Middle Layer	-0.628 0.164	-
Bottom Layer	-1.451 0.000	-0.823 0.045

Appendix E: Vector Magnitude

Table 5.12: CMHB: ANOVA results for Vector magnitude.

Source of Variation	Sum of Squares	df	Mean Squares	F value	Prob. > F value	$F_{critical}$
Between Groups	7.640	2	3.820	0.16	0.856	3.068
Within Groups	3560.252	145	24.553	-	-	-
Total	3567.891	147	-	-	-	-

Table 5.13: PFC: ANOVA results for Vector magnitude.

Source of Variation	Sum of Squares	df	Mean Squares	F value	Prob. > F value	$F_{critical}$
Between Groups	32.447	2	16.224	0.54	0.584	3.068
Within Groups	4356.796	145	30.049	-	-	-
Total	4389.244	147	-	-	-	-

Table 5.14: Superpave: ANOVA results for Vector magnitude.

Source of Variation	Sum of Squares	df	Mean Squares	F value	Prob. > F value	$F_{critical}$
Between Groups	288.458	2	144.229	8.63	0.000	3.068
Within Groups	2423.340	145	16.713	-	-	-
Total	2711.797	147	-	-	-	-

Table 5.15: Superpave: Scheffe results for Vector Magnitude.

Row Mean - Col. Mean	Top Layer	Middle Layer
Middle Layer	1.072 0.433	-
Bottom Layer	3.340 0.000	2.268 0.024

Appendix F: Modified Vector Magnitude

Table 5.16: CMHB: ANOVA results for Modified Vector magnitude.

Source of Variation	Sum of Squares	df	Mean Squares	F value	Prob. > F value	$F_{critical}$
Between Groups	65.811	2	32.906	0.19	0.824	3.068
Within Groups	24649.330	145	169.995	-	-	-
Total	24715.141	147	-	-	-	-

Table 5.17: PFC: ANOVA results for Modified Vector Magnitude.

Source of Variation	Sum of Squares	df	Mean Squares	F value	Prob. > F value	$F_{critical}$
Between Groups	211.518	2	105.759	0.40	0.669	3.068
Within Groups	38050.984	145	262.421	-	-	-
Total	38262.501	147	-	-	-	-

Table 5.18: Superpave: ANOVA results for Modified Vector Magnitude.

Source of Variation	Sum of Squares	df	Mean Squares	F value	Prob. > F value	$F_{critical}$
Between Groups	52.613	2	26.307	0.46	0.631	3.068
Within Groups	8258.840	145	56.957	-	-	-
Total	8311.450	147	-	-	-	-

Appendix G: Aggregate Equivalent Diameter

Table 5.19: CMHB: ANOVA results for Equivalent Diameter.

Source of Variation	Sum of Squares	df	Mean Squares	F value	Prob. > F value	$F_{critical}$
Between Groups	9.206	2	4.603	1.44	0.242	3.100
Within Groups	339.010	95	3.198	-	-	-
Total	348.216	97	-	-	-	-

Table 5.20: PFC: ANOVA results for Equivalent Diameter.

Source of Variation	Sum of Squares	df	Mean Squares	F value	Prob. > F value	$F_{critical}$
Between Groups	5.988	2	2.994	1.18	0.310	3.100
Within Groups	273.182	95	2.529	-	-	-
Total	279.170	97	-	-	-	-

Table 5.21: Superpave: ANOVA results for Equivalent Diameter.

Source of Variation	Sum of Squares	df	Mean Squares	F value	Prob. > F value	$F_{critical}$
Between Groups	3.093	2	1.547	2.55	0.080	3.100
Within Groups	182.825	95	0.607	-	-	-
Total	185.919	97	-	-	-	-